To the Graduate Council:

I am submitting herewith a thesis written by Charles F. Leonard entitled "Analytical and Experimental Study of Flow Between A Smooth Rotor and Stator." I recommend that it be accepted in partial fulfillment of the requirements for the degree of Master of Science, with a major in Mechanical Engineering.

William S. Johnson, Major Professor

We have read this thesis
and recommend its acceptance:

Accepted for the Council:

Vice Chancellor
Graduate Studies and Research

A

Thesis
80
.L465
cop. 2

ANALYTICAL AND EXPERIMENTAL STUDY OF FLOW BETWEEN A SMOOTH ROTOR AND STATOR

A Thesis

Presented for the

Master of Science

Degree

The University of Tennessee, Knoxville

Charles F. Leonard

March 1980

1116261

ACKNOWLEDGMENTS

The author is indebted to many persons too numerous to mention. However, a few special thanks need to be given. First, very special thanks should be given to Dr. W. S. Johnson for help in preparation of this thesis.

A expression of gratitude needs to be given to J. R. Missimer, who was a good sounding board for new ideas.

The author wishes to express appreciation to the people who work in the Mechanical and Aerospace Engineering Shop.

Finally, a very deep thanks and love to my family, and especially to my mother who typed the many rough drafts of my thesis.

ABSTRACT

The main purpose in this study was to collect pressure and localized shear stress data for laminar flow of a constant property Newtonian fluid across two parallel smooth rings positioned extremely close to each other. In particular, the case where one of the rings was attached to a rotating disk and the other was attached to a stationary disk. The pressure and its distribution were obtained from pressure taps located in the stator. The tangential shear stresses on the stator were obtained by a flush mounted surface probe.

Along with showing what certain physical parameters did to pressure and shear stresses, analytical expressions for pressure distribution, shear stress, and flow rates giving zero pressure difference between the plenum in the test rig and ambient conditions.

TABLE OF CONTENTS

CHAPTER		PAGE
I.	INTRODUCTION	1
	A. General	1
	B. Statement of Problem	4
	C. Method of Study	6
II.	DEVELOPMENT OF BASIC EQUATIONS	7
III.	EXPERIMENTAL APPARATUS AND CALIBRATION	15
	A. General	15
	B. Test Rig	15
	C. Calibration	22
IV.	EXPERIMENTAL PROCEDURES	28
V.	THE THERMO-SYSTEM 1237W FLUSH SURFACE PROBE	30
VI.	ANALYTICAL AND EXPERIMENTAL RESULTS	34
	A. General	34
	B. Pressure	34
	C. Surface Shear Stress	46
	D. Zero Pressure Difference	52
	E. Assumption of Axisymmetry	54
VII.	CONCLUSIONS	56
VIII.	RECOMMENDATIONS	60
LIST OF REFERENCES		61
APPENDICES		63
APPENDIX A.	DERIVATION OF GOVERNING EQUATIONS	64
APPENDIX B.	DERIVATION OF MOMENT OF MOMENTUM EQUATION	73
APPENDIX C.	FLOW REGIME	75

CHAPTER PAGE

APPENDIX D. DATA UNCERTAINTY ANALYSIS 77

APPENDIX E. COMPUTER PROGRAM 81

APPENDIX F. DATA 84

APPENDIX G. CALIBRATION PROCEDURE FOR SURFACE PROBE 97

APPENDIX H. DERIVED EXPRESSIONS 98

VITA 103

LIST OF TABLES

TABLE		PAGE
1.	Pressure Uncertainty (in Inches of Water) vs. Flow Location . .	80
2.	Average Pressure Data in Inches in Water	84
3.	Averaged Tangential Shear Stress Data in Volts	88
4.	Averaged Radial Shear Stress Data in Volts	91
5.	Averaged Zero Pressure Difference Data Pressure in Inches of Water Flow Rates in SCFH (Q)	94
6.	Averaged Zero Pressure Difference Data Pressures in Inches of Water Flow Rates in SCFH (Q)	95
7.	Directional Data from Flush Surface Probe in Volts	96

LIST OF FIGURES

FIGURE		PAGE
1.	Typical Rotor and Stator Configuration for a Clutch	2
2.	Flow in a Disengaged Clutch	5
3.	Cylindrical Coordinate System	9
4.	Control Volume for Analytical Model	12
5.	Experimental Apparatus	16
6.	Stator	18
7.	Test Rig	20
8.	Inclined Manometers	20
9.	Air Flow Meters	21
10.	Thermo-Systems 1237W Flush Surface Probe	23
11.	Thermo-Systems Supply and Monitor	24
12.	Probe Mount	31
13.	Comparison of Measured and Analytically Predicted Pressure Distributions I	35
14.	Comparison of Measured and Analytically Predicted Pressure Distributions II	37
15.	Analytical Prediction of Pressure Profile	38
16.	Comparison of Radial Pressure Distribution with Experimental Data	40
17.	The Influence of Rotational Speed on Pressure	41
18.	The Influence of Gap on Pressure	42
19.	Comparison of the Analytical Prediction of Pressure with Experimental Data I	44

FIGURE PAGE

20. Comparison of Analytical Prediction of Pressure with Experimental Data II. 45

21. Comparison of Experimental Data for Shear Stress Distribution with Analytical Prediction. 48

22. Comparison of Average Shear Stress to the Analytical Predicted Average. 50

23. Comparison of Analytical Predicted Shear Stress Profile with Experimental Data 51

24. Comparison of Analytically Predicted Flow Rate for Zero Pressure Difference with Experimental Data 53

25. Relative Positions of Pressure Taps and Table 55

26. Hot Film Surface Probe Calibration Curve. 58

NOMENCLATURE

Q	volumetric flow rate of air
u	radial velocity
v	tangential velocity
P	pressure
θ	angular velocity of rotating disk
r	radial coordinate
z	spatial coordinate perpendicular to stator
g	distance between disks (gap width)
ρ	density of air
μ	dynamic viscosity of air
A	coefficient in tangential velocity profile
B	coefficient in tangential velocity profile
C	coefficient in tangential velocity profile
$\dot{m}$	mass flow rate of air
τ	shear stress
τ_s	shear stress on stator
τ_r	shear stress on rotor
r_o	outside radius of disk (or of ring)
r_i	inside radius of ring
$1/Pv$	Reynolds No. in tangential direction ($\frac{V_o r_o}{}$)
Re	Reynolds No. in radial direction ($\frac{U_o r_i}{V}$)
Re_Q	Reynolds No. Based on Q ($\frac{U_o g}{}$)
Rr	gap to radius ratio (g/r_o)
θ	ratio inside radius of ring to outside radius of ring (r_i/r_o)

U_o characteristic radial velocity $(\frac{Q}{2\pi g r_1})$

V_o characteristic tangential velocity $(r_o\theta)$

T torque on control volume or rings

P_o characteristic pressure

CHAPTER I

INTRODUCTION

A. General

The flow of oil or air to cool a disengaged clutch, the pressure distribution in a seal, and the process of manufacturing records are all examples of situations that could be modeled as fluid flowing between a closely spaced rotor and stator. Therefore, research on this type of flow field has practical as well as academic importance. This investigation studied the radial flow of a constant property Newtonian fluid between two smooth closely spaced rings mounted on disks (Figure 1). Investigations on similar types of flow regimes has taken many forms from elaborate computer modeling, to making assumptions that reduce the Navier-Stokes equations to a form that can be solved in closed form. There are many examples of the above techniques: for instance, an integral analysis of flow in a disengaged clutch that models a rotor with radial grooves, has been developed by J. R. Missimer in a dissertation entitled "Analytical Model of Flow Between Smooth Stationary Disc and Grooved Rotating Discs,"[1] at the University of Tennessee, Knoxville. The investigation team of Bayley and Owens[2] studied the effects of a turbulent radial outflow superimposed upon the motion of the fluid between a rotating and stationary plane disk. They developed the governing equations for this flow by taking the Navier-Stokes equations and performing an order-of-magnitude evaluation to reduce them to boundary layer form. Basically, the only assumption they made in the order-of-magnitude analysis was that the gap width was much less than the radius of the two disks. Bayley and Owens

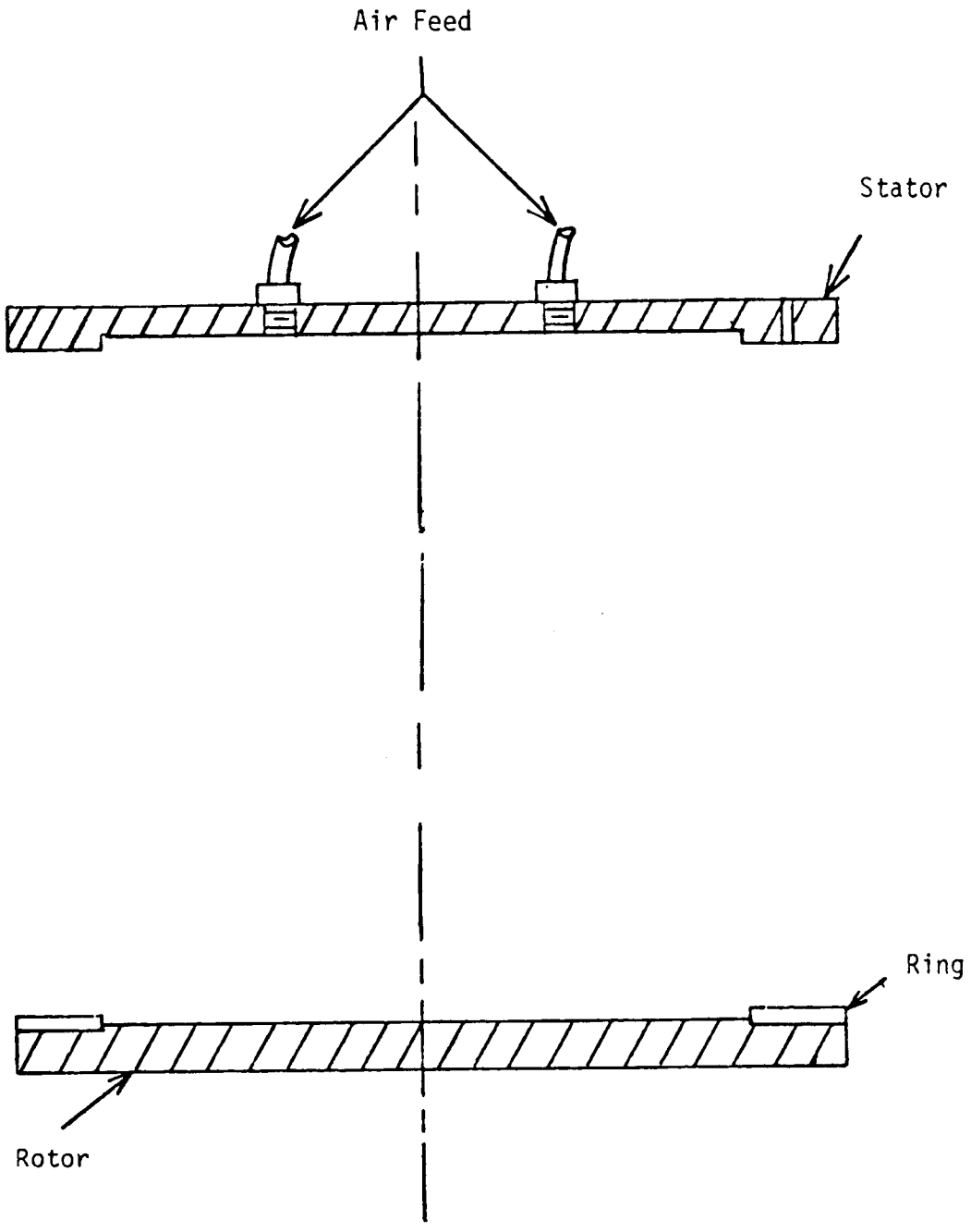


Figure 1. Typical Rotor and Stator Configuration for a Clutch.

had to depend on special numerical methods to solve their governing set of equations. There was another team of investigators, Pelech and Shapiro,[3] who examined the problem of a thin flexible disk rotating next to a flat plate with fluid flowing radially outward. Pelech and Shapiro were able to obtain a closed form solution to their problem by using an order-of-magnitude analysis. In this order-of-magnitude analysis two assumptions were made. The first assumption was that the velocity in the tangential direction was much greater than the velocity in the radial direction. Secondly, they assumed that the gap width was much less than the radius of the disk. By using an order-of-magnitude analysis, Pelech and Shapiro obtained a pressure, viscous and centrifugal force balance in the radial momentum equation, i.e., negligible inertia forces. The basic equation they obtained is given by the following (Appendix A):

$$\frac{\partial^2 U}{\partial z^2} = \frac{1}{\mu}\frac{dP}{dr} - \frac{\rho}{\mu}\frac{V^2}{r} \qquad (1)$$

and the assumed couette velocity profile is given by:

$$V = \left(\frac{z}{g}\right)\dot{\theta}r \quad . \qquad (2)$$

After substituting Equation (1) into Equation (2), they achieved a closed form solution for the pressure distribution by direct integration.

Flow in a disengaged clutch has several different characteristics than the problem addressed by Pelech and Shapiro. For example, in a disengaged clutch, fluid may be injected through the center of the stator. Since the disks in a clutch have rings mounted on each facing

surface (Figure 1), the analysis is usually begun by assuming that the flow is purely radial until it reaches the rings, where it acquires a tangential velocity (Figure 2). By assuming a couette profile for the tangential velocity, one requires that the tangential shear stresses are the same on both the rotor and stator. It is even though by some investigators that the tangential shear stresses do not vary with radius on the stator.[2] However, it is now believed that there are radial variations in the tangential shear stresses. In fact, it can be shown, by application of the moment of momentum principle,[4] that there are differences in the tangential shear stresses between the rotor and stator due primarily to the acceleration on the fluid across the ring (Appendix B).

A linear velocity profile for the tangential velocity fails to predict one flow phenomenon, namely that of differentiating shear (tangential) stresses between that of the rotor and stator. A quadratic profile in the axial direction, where the coefficients are functions of the radius, instead of a linear profile would better account for this phenomenon. This quadratic profile, like the linear profile would also allow tangential shear stresses to vary in the radial direction on the stator.

B. Statement of Problem

This investigation studied the laminar flow of a constant property Newtonian fluid across two smooth rings positioned extremely close to each other. In particular, this investigation looked at the case where one of the parallel rings was attached to a stationary disk, while the other ring was attached to a rotating disk (Figure 1). The

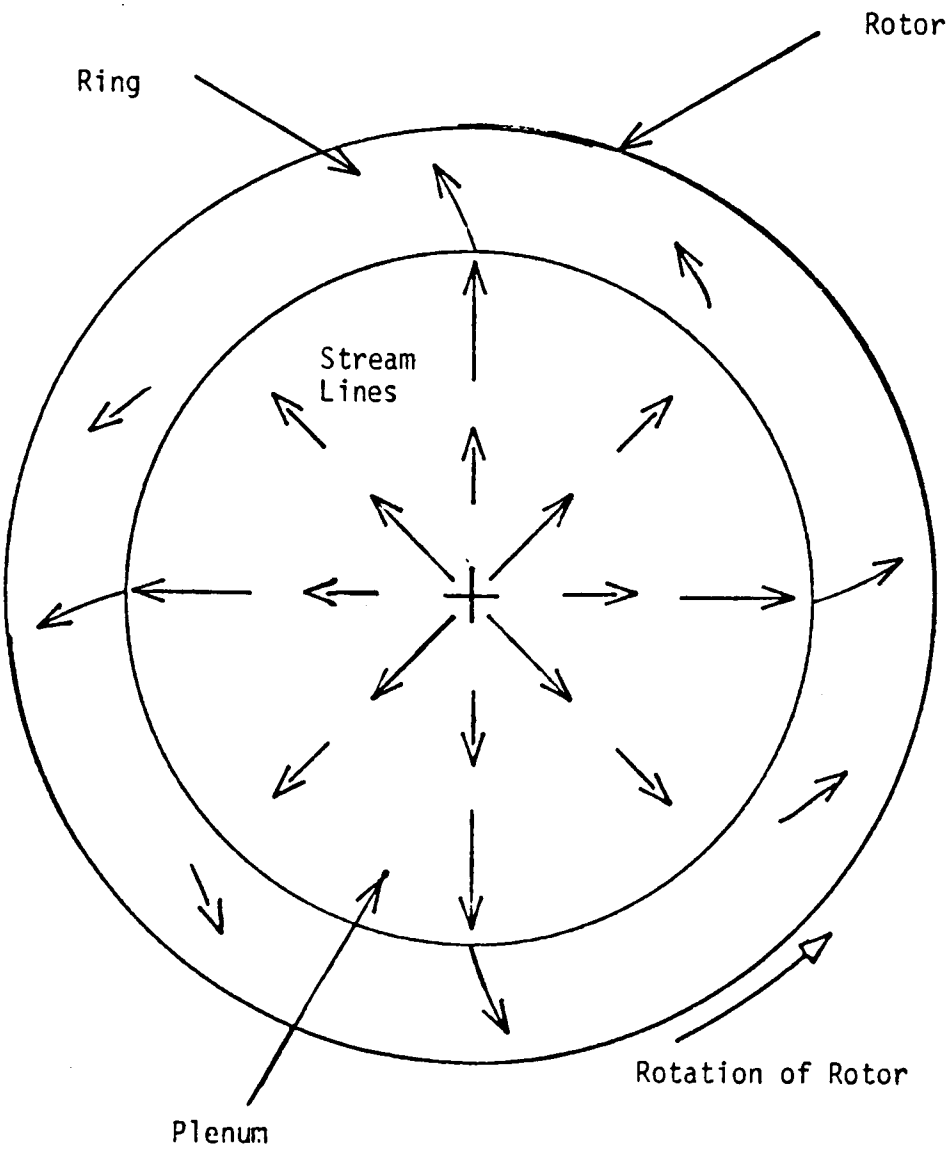


Figure 2. Flow in a Disengaged Clutch.

study investigated various ratios of tangential velocities to radial velocities and various gap widths to radial length ratios.

C. Method of Study

Since the assumption of a couette velocity profile leads to certain inaccuracies in predicting shear stresses on the rotor and stator, it was proposed to take Pelech and Shapiro's basic governing equations and assume a quadratic velocity profile for the tangential velcoity distribution in the axial direction. This was done in an effort to extend the range over which the basic assumptions could be applied and to better account for tangential shear stress differences between the rotor and stator. Experimental data was collected to verify the predictions made by the expressions obtained from the quadratic analysis.

CHAPTER II

DEVELOPMENT OF BASIC EQUATIONS

When approaching a new fluid dynamic problem an investigator usually starts with the general form of the Navier-Stokes equations and then proceeds to simplify these equations. The simplification is usually done by eliminating terms which are small for the particular problem of interest. Bayley and Owens have studied the flow between a smooth rotating disk and a closely spaced smooth rotor and have presented a simplified form of the momentum and continuity equations for such a situation. However, there are other sets of momentum and continuity equations. Pelech and Shapiro proposed one such set. By imposing certain conditions on the tangential and radial velocities as well as the gap and radius ratios, they were able to simplify the Navier-Stokes equation to a expression that had a closed form analytical solution.

In this analysis two assumptions about the flow were also made. The first assumption was that the characteristic length in the radial direction (z) was negligible compared to the radial characteristic length (R_o), that is,

$$\frac{z_o}{R_o} << 1 \tag{3}$$

and that the characteristic radial velocity (U_o) was also negligible compared to the tangential velocity (V_o), that is

$$\frac{U_o}{V_o} << 1 \tag{4}$$

Applying these assumptions to the procedures used in simplifying the Navier-Stokes equations, the simplified form reduces to the following set of equations (governing equations)(Appendix A):

$$-\frac{V^2}{r} = -\frac{1}{\rho}\frac{dP}{dr} + V\frac{\partial}{\partial z}\left[\frac{\partial U}{\partial z}\right] \tag{5}$$

$$0 = \frac{\partial^2 V}{\partial z^2} \tag{6}$$

$$0 = \frac{1}{r}\frac{\partial(rU)}{\partial r} + \frac{\partial w}{\partial z} \tag{7}$$

The cylindrical coordinate system was attached to the stator to ensure an inertial coordinate system (Figure 3). The above set of equations are subject to the following boundary conditions:

$$u(r, o) = 0 \tag{8}$$

$$u(r, s) = 0 \tag{9}$$

$$v(r, o) = 0 \tag{10}$$

$$v(r, g) = r\dot{\theta} \tag{11}$$

$$w(r, o) = 0 \tag{12}$$

$$w(r, s) = 0 \tag{13}$$

Boundary conditions 8-11 are non-slip conditions that must be met at the wall. Conditions 12 and 13 represent no mass flux through the stator and rotor surfaces, respectively.

Non-dimensionalizing the governing equations resulted in the appearance of the following non-dimensional parameters:

$$Re = \frac{Qr_o}{2\pi v r\, gv} \tag{14}$$

$$Pv = \frac{r}{\theta r_o g} \tag{15}$$

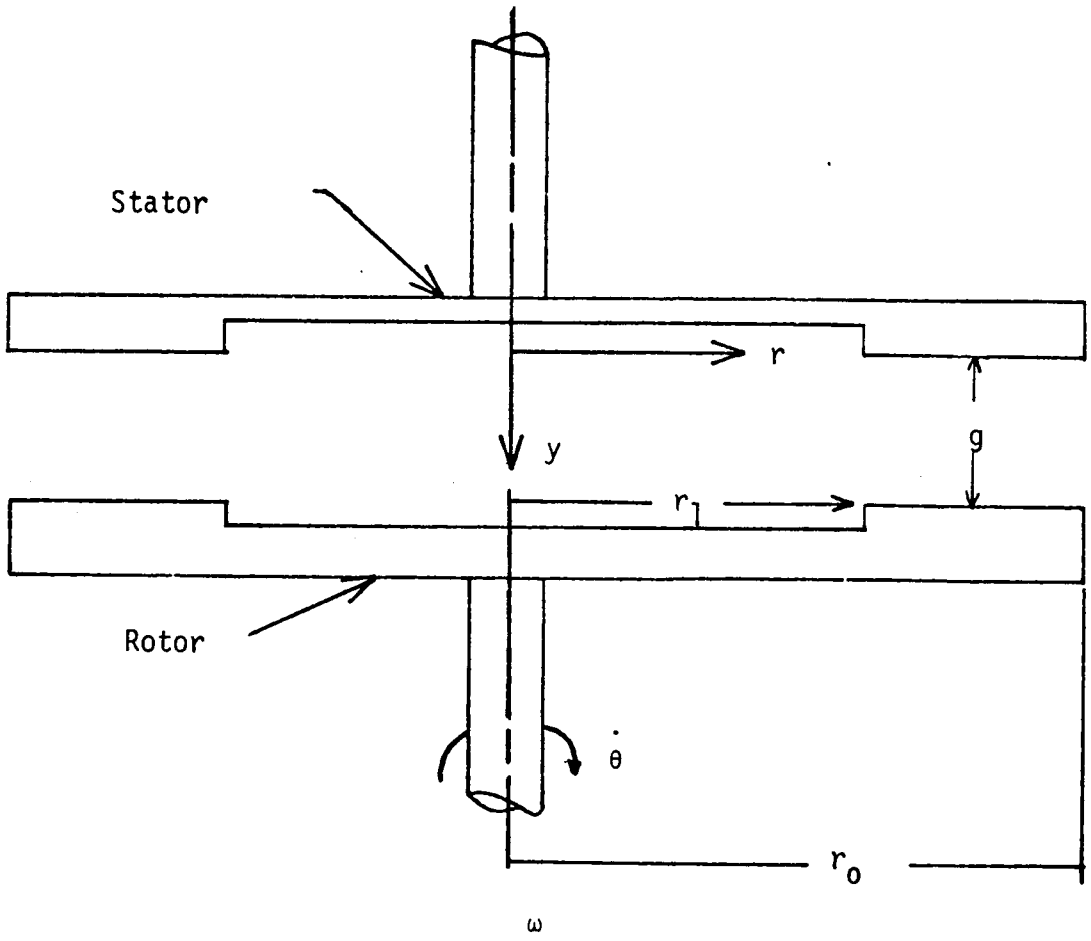


Figure 3. Cylindrical Coordinate System.

$$Rr = g/r_o \tag{16}$$

$$\theta = r_i/r_o \tag{17}$$

Re is a Reynolds number based on radial flow of air. $\frac{1}{Pv}$ can be thought of as a Reynolds number for flow in the tangential direction. R_r, the gap ratio, is defined as the ratio of the gap width to the outside radius. The radius ratio, θ, is simply the ratio of the radius of the inner ring of the test section to the radius of the outer ring. This is the only parameter that was held constant during the investigation.

Equation 6 in the set of governing equations was also obtained by Pelech and Shapiro. This equation indicates a linear velocity profile for the tangential velocity distribution profile with respect ot the axial coordinate (z). Pelech and Shapiro had good success in predicting the pressure distribution for small gaps in the range of 10^{-3} inches. However, at larger gaps, 10^{-2} inches, more angular momentum is imparted to the flow and the difference between the tangential shear stresses on the rotor and stator becomes larger. In an effort to empirically account for these added flow phenomena at larger gaps, a quadratic profile, instead of a couette one, was assumed. The intent of the quadratic profile was to empirically expand the basic analysis to larger gaps. The quadratic tangential velocity profile is given by:

$$B = A + Bz + Cz^2 \quad . \tag{18}$$

The coefficients in this tangential velocity profile were determined by applying the boundary conditions. The first coefficient, A, in the above equation, can be solved by noting the boundary condition V (r, o) = 0. The second and third coefficients, B and C, may be

related to each other by the boundary condition $V(r, g) = r\dot{\theta}$. This relationship is given by:

$$Bg + Cg^2 = r\dot{\theta} \quad . \tag{19}$$

A third condition was needed to solve for B and C. This condition was obtained by the application of the moment of momentum (Euler's Turbine)[4] equation,

$$T = \dot{m}(V_{\theta_{out}} r_{out} - V_{\theta_{in}} r_{in}) \quad . \tag{20}$$

This T is the net torque transferred from the rotor to the stator. It may also be viewed as the torque applied to a control volume whose boundaries are the two disks and inner and outer radii of the test ring (Figure 4). The torques on the disk are found by integrating the tangential shear stresses over the area of the test rings. The tangential shear stress on the rotor is given by:

$$\tau_r = \mu(b + 2\,Cg) \tag{21}$$

and the tangential shear stress on the stator is given by:

$$\tau_s = \mu b \quad . \tag{22}$$

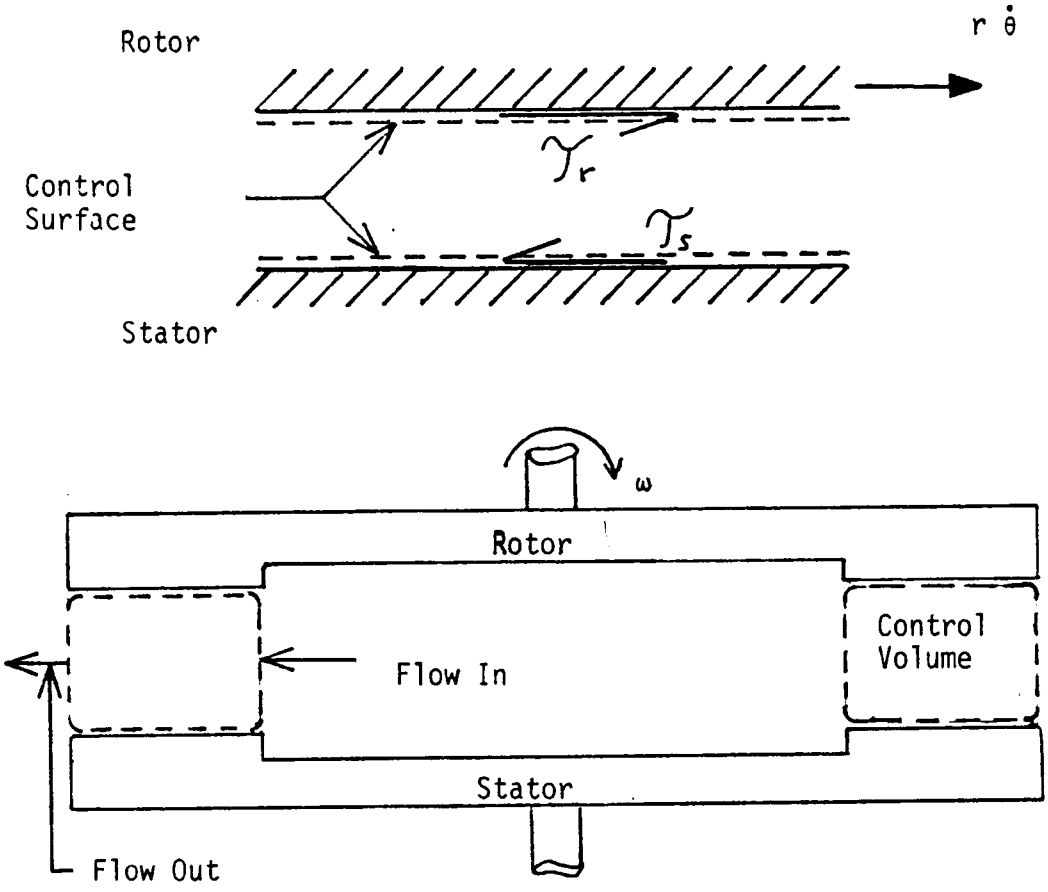
Thus the net differential torque applied to the control volume is given by:

$$\mu(b + 2Cg - b) = \mu 2Cg \tag{23}$$

Equations 20 through 23 may be combined and arranged to give a differential equation for C. This differential equation,

$$\frac{dC}{dr} + C\left(\frac{1}{r} + \frac{24\tau\mu}{g\rho Q}\right) = \frac{6\dot{\theta}}{g^2} \quad , \tag{24}$$

is a first order linear ordinary differential equation with variable coefficients, requiring one boundary condition on C. From the work



$\tau_r =$ Shear Stress Caused by Rotor

$\tau_s =$ Shear Stress Caused by Stator

Figure 4. Control Volume for Analytical Model.

done by J. R. Missimer,[1] who assumed that the tangential velocity profile could be approximated as couette near the stator's wall, comes the boundary condition on C. Missimer assumed that the non-dimensionalized velocity at the inner radius of the ring was half of the rotor's speed at the inner radius. Therefore, the profile was assumed to be close to a couette profile. These assumptions lead to the boundary condition that C = 0 at the inner radius of the ring. By using an integrating factor, C was solved for and is given by:

$$C = \frac{\dot{\theta}\rho Q}{4\pi\mu g}\left(\frac{1}{r}\right)\left(1-\exp\left(\frac{12\tau\mu}{g\rho Q}(r_i^2 - r^2)\right)\right) \qquad (25)$$

Two items should be noted about the coefficients B and C. First, they are both functions of the radius. Secondly, B may be dropped out of the velocity distribution, as was also done in the differential torque equation, by making the substitution:

$$b = \frac{r\dot{\theta}}{g} - Cg \qquad (26)$$

Thus the tangential velocity distribution becomes

$$V = bz + Cz^2 = r\dot{\theta}\left(\frac{z}{g}\right) + C(z^2 - gz) \qquad (27)$$

Substituting this velocity distribution into the set of governing equations (5-7), one obtains the following expressions for $\frac{dP}{dr}$, τ_s, and V (Appendix I).

Derived expressions:

$$\frac{dP}{dr} = \frac{6Q\mu}{\pi g^3 r} + \rho\left(\frac{3r\dot{\theta}}{10} + C\left(-\frac{g^2}{5} + \frac{3g^4 C}{7 \text{ or } 6}\right)\right) \qquad (28)$$

$$\tau_s = \mu\left(\frac{r\dot{\theta}}{g} - \frac{\dot{\theta}\rho Q}{4\pi\mu g}\right)\left(\frac{1}{r}\right)\left(1-\exp\left(\frac{12\pi\mu}{g\rho Q}(r_i^2 - r^2)\right)\right) \qquad (29)$$

$$V = r\dot{\theta}\left(\frac{z}{g}\right) - \frac{\dot{\theta}\rho Q}{4\pi\mu g}\left(\frac{1}{r}\right)\left[1-\exp\left[\frac{12\pi\mu}{g\rho Q}\left(r_i^2 - r^2\right)\right]\right] \qquad (30)$$

To solve for the pressure distribution, numerical techniques had to be employed. It was decided to use CSMP, a user-oriented computer language,[6] to obtain the pressure distribution from the ordinary differential equation.

CHAPTER III

EXPERIMENTAL APPARATUS AND CALIBRATION

A. General

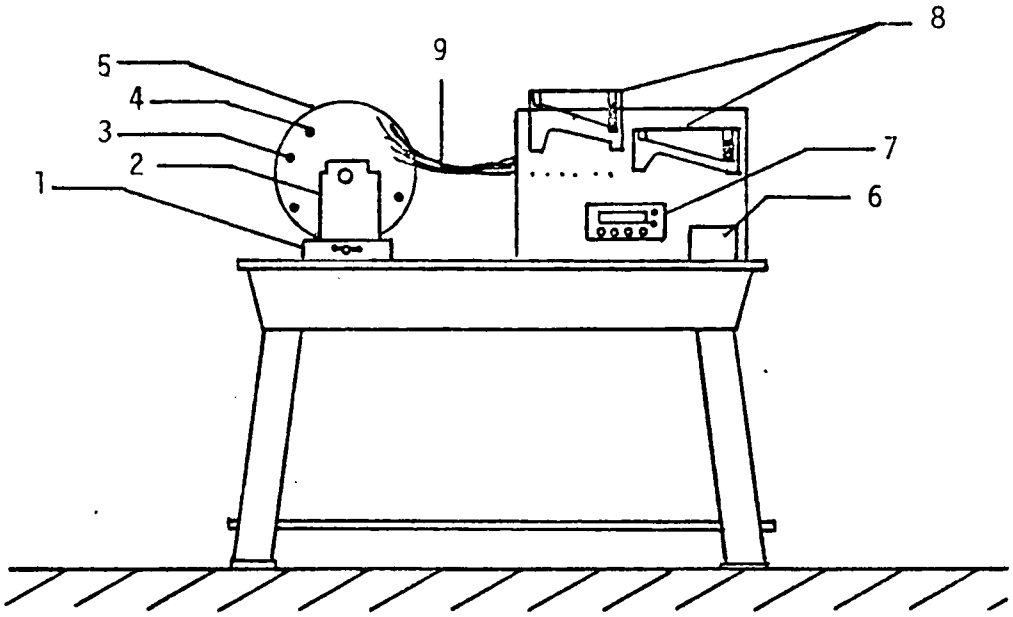
The accuracy of the equations derived from the quadratic profile needed to be verified by experimental data. Since no data existed, experiments were conducted to acquire such data. A test rig was designed and constructed to accomplish this task. Along with this test rig, equipment was needed to monitor experimental variables and to collect the data. A detailed description of the test rig, the support system and the data acquisition system is given below.

B. Test Rig

The test rig was located in room M-7 of Doughtery Hall on the University of Tennessee, Knoxville campus. The apparatus consisted of two smooth rings mounted on two plane disks, a stator and a rotor, which was attached to a 3 ft x 3 ft cast iron table. The rotor was spun by a motor-belt-spindle arrangement. Air was injected through the stator from the building's air supply system after passing through two filters. The flow rates of air were measured by two air rotameters (Figure 5).

1. Disks

The stator and the rotor were machined out of 1 inch aluminum sheets into disks having an outside diameter of 15 inches. The design on the stator called for it to be cut down to 3/4 of an inch thick with a 1/4 inch step placed at a radius of 5.85 inches. This placed the test



No.	Item
1.	Graduated Slide
2.	Disk Support
3.	Depth Gage
4.	Probe Hole
5.	Disk
6.	Motor Control
7.	Speed Indicator
8.	Inclined Manometer
9.	Pressure Tubes

Figure 5. Experimental Apparatus.

region on the stator between a radius of 5.85 and 7.50 inches. The step also created a plenum in the central region of the two disks. This plenum acted as a damper to any flow pertubations. Ten pressure taps were placed in the stator at radii of 3.00, 5.905, two at 6.265, 6.675, 7.088, 7.253, 7.335, 7.368, and 7.41 inches. (The two pressure taps at 6.265 inches were used to check the axisymmetric condition, and is discussed later in Chapter VI, Section E.) The mounting holes for the hot film surface probe (see Section 3, Chapter III) were located in the stator at radii of 6.40, 6.675, and 6.95 inches. The air was symmetrically injected through the stator by two holes which were four inches apart. Two air holes were needed in the stator so that enough air could be injected into the test rig. The use of one big air intake was avoided because of support reasons for the stator. To have a reliable way of measuring the spacing between the rotor and the stator a micrometer was mounted on the stator (Figure 6).

To maintain proper alignment of the rotor and stator, the stator was mounted on a slide. By adjusting the slide the stator could be moved axially changing the spacing between the two disks (i.e. the gap distance) and still remain parallel to the rotor.

Before the rotor and spindle were secured to the table, they were placed in a lathe where the ring or the rotor assembly was faced off to ensure proper alignment about the rotor spin axis (z). The ring on the rotor also had an inner radius of 7.5 inches, thus the test sections were the same on both the rotor and stator.

Unlike the stator, the rotor consisted of two parts, a detachable ring and a disk. This increased the test rigs capability of gathering a

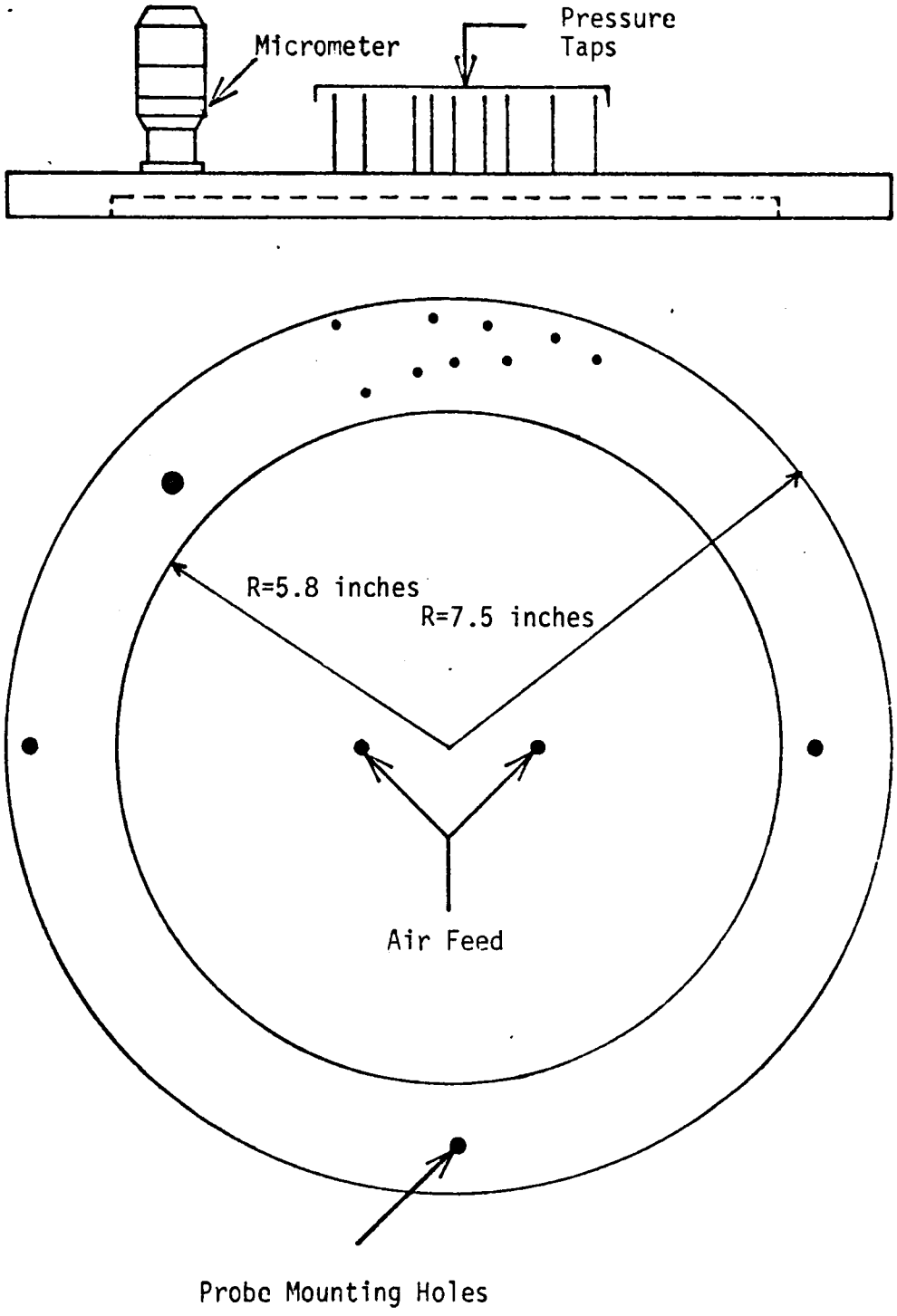


Figure 6. Stator.

variety of data on other parameters, such as a rotor whose face had machined grooves in it. The rotor assembly was mounted on a spindle, manufactured by Whitnon Manufacturing Company, and then bolted to the cast iron table (Figure 7).

2. Support System

A General Electric variable speed motor rated at 5 H.P., which also had a maximum speed of 3500 RPM, was used to turn the rotor. A magnetic pick-up connected to a Monsanto Counter monitored the Angular velocity of the rotor. Because the counter's digital output displaced the speed of the rotor directly in RPM's, the speed could be continuously monitored and/or corrected during experimental testing (Figure 8).

The air that was injected into the test rig was taken from the building air supply after passing it through two filters and through two Dwyer Visi-Float Flowmeters which were connected in parallel to the test apparatus. These two rotameters were calibrated in standard cubic feet per hour (SCFH). Since the experiment calls for air flow ranging from 0-500 SCFH, two sets of rotameters were used. The capacity of the rotameters used was from 0-20 SCFM incremented in 1 SCFH and from 20-300 incremented in 5 SCFH (Figure 9).

3. Data Acquisition System

The data acquisition dealt mainly with obtaining two kinds of data: radial pressure distributions and surface shear stresses on the stator. Pressure distributions were obtained by recording individual pressures from the pressure taps located in the test region of the rotor. The pressures were measured by a Dwyer oil-filled inclined manometer

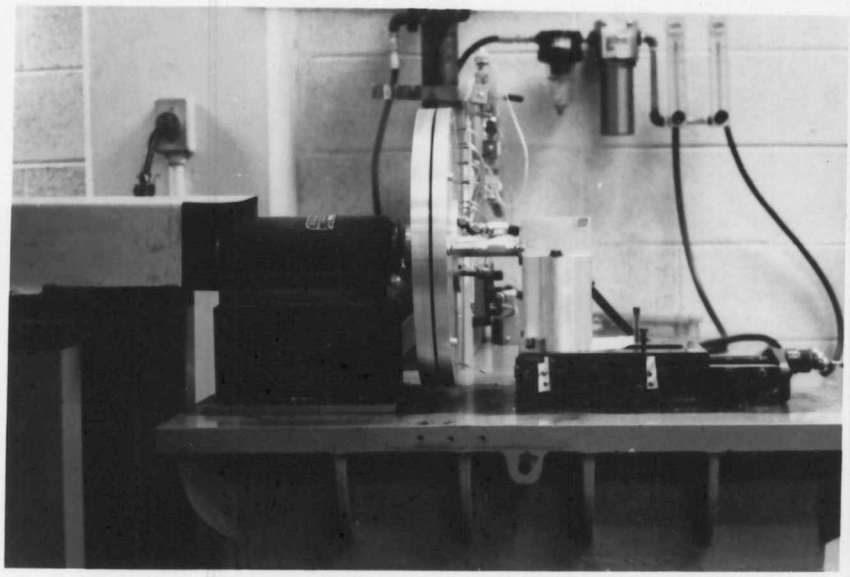


Figure 7. Test Rig.

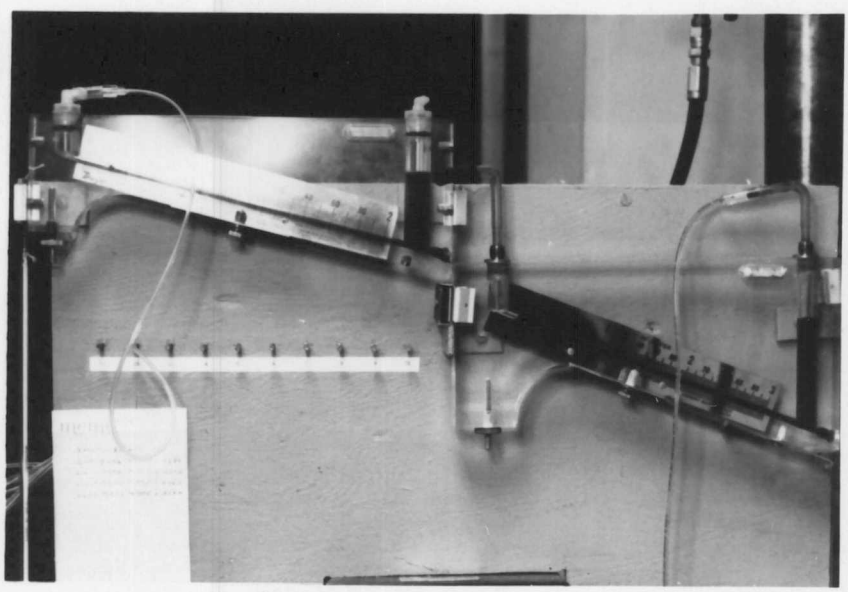


Figure 8. Inclined Manometers.

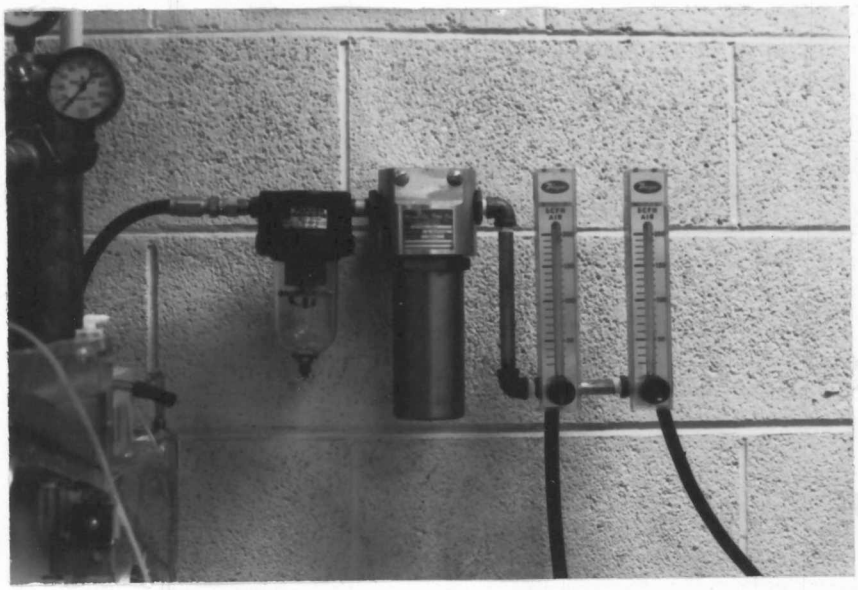
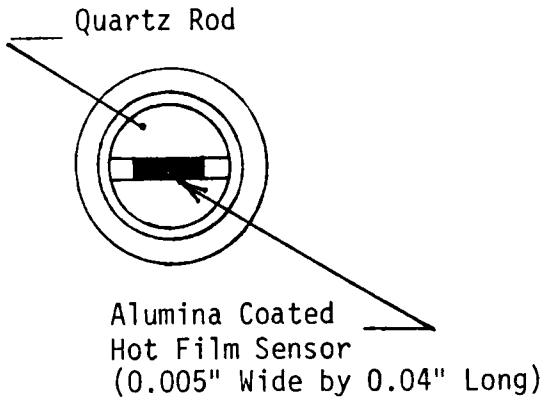


Figure 9. Air Flow Meters.

which was calibrated in inches of water and incremented in hundredths of an inch. Because the investigation dealt only with steady state conditions, all of the pressures could be obtained from one manometer. The other data required for experimental verification of expressions obtained from the quadratic velocity profile were surface shear stresses. Therefore, a means of measuring the stresses on the stator was essential. A literature search revealed that a flush mounted hot film surface probe could adequately measure surface shear stresses when air is the fluid medium.[7-10] The probe used to measure the surface shear stresses was a 1237W Flush Surface Probe manufactured by Thermo-Systems, Inc. (Figure 10). The end of the probe was made flat so that when it was mounted properly no flow disturbance was introduced. The sensor in the probe was made from an aluminum coated platinum strip measuring 0.005 inches wide by 0.040 inches long. A stainless steel rod acted as a shield to a quartz rod that had the sensor embedded in its end. The rod measured 0.125 inches wide and 1.50 inches long. The instrumentation used to power and monitor the probe was a Thermo-Systems Monitor and Supply Series 1050 and a Data Precision voltmeter (Figure 11).

C. Calibration

The validity of any experimental study is only assured after the instruments used in measuring important parameters and experimental data have been calibrated. There exists several methods for calibrating equipment. One way is to calibrate against some theoretical predictions. The second way is to use some standard that has been previously calibrated.



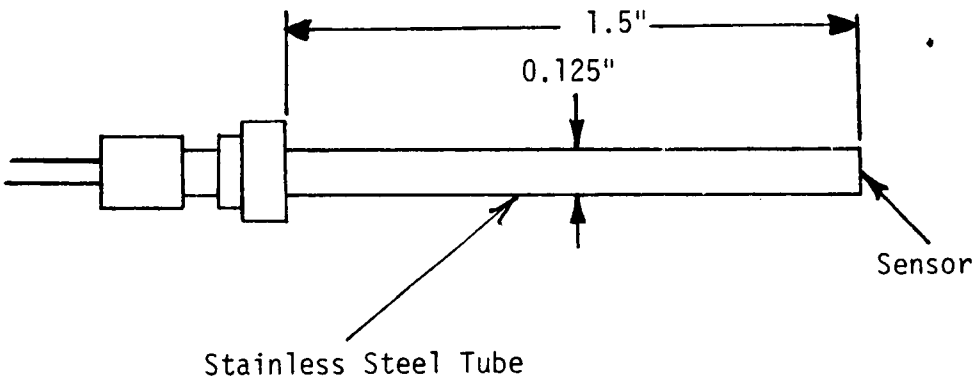


Figure 10. Thermo-Systems 1237W Flush Surface Probe.

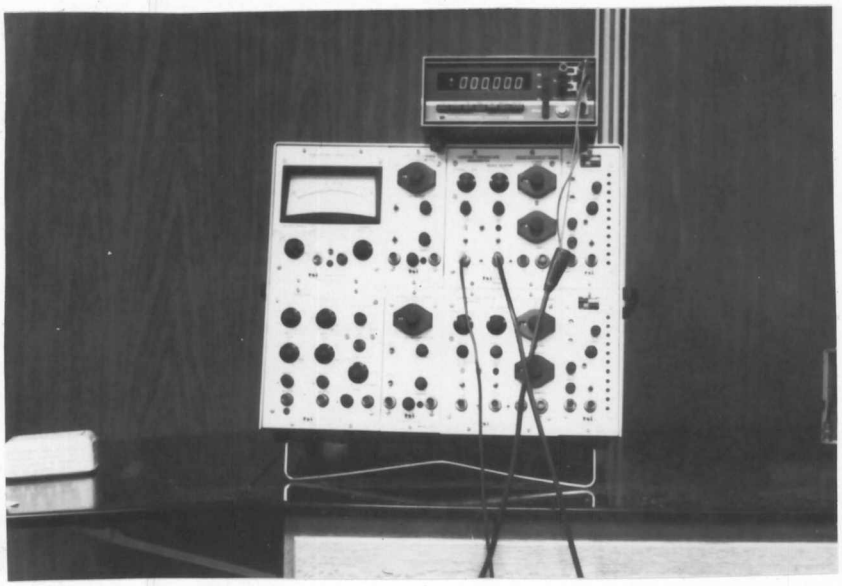


Figure 11. Thermo-Systems Supply and Monitor.

Some equipment may only have to be calibrated once during an investigation, while others should be calibrated many times during an experiment.

The magnetic pickup counter system was an example of an instrument that only needed to be adjusted once during the experiment. Since the sensitivity of the magnetic pickup was primarily a function of the distance between its probe and the teeth on the shaft connecting the rotor to the motor, the counter was set for the entire experiment after the gap had been adjusted once. The counter was calibrated, i.e., the gap set, by two instruments, a stroboscope and a tachometer. By matching the two outputs, the counter against the stroboscope or tachometer, indicated the need adjustment of the probe.

It was imperative that the two disks remain parallel during the investigation. This was checked regularly during the experiment. To check the alignment, a micrometer was mounted on the rotor. Thereby rotating the rotor in 90° increments the alignment could be checked. At each position of the rotor the micrometer was read to an accuracy within one half of a thousandth of an inch. All other measurements were also held to within the same limits.

Since the test section on the rotor was a ring attached by eight screws, there was a tendency for the test surface to warp. This condition was checked by using the micrometer mounted in the stator. By using the micrometer the same way it was used to check the gap setting, the surface variation on the rotor could be checked. By rotating the rotor and measuring the gap at eight different tangential positions, the gap could be set. The deviation of the eight different gap readings was used to obtain the surface variation. The maximum allowable variation

was less than $\pm$ 0.0005 of an inch. When this limit was exceeded, the spindle and rotor assembly were taken to the shop and the test surface was machined back into tolerance.

The hot film surface probe was checked against theoretical predictions instead of another instrument. A procedure for calibrating the surface probe had to be developed since there was no equipment available to perform this task. By maintaining the two 15 inch disks stationary and shrinking the gap between them to 0.010-0.020 inches, the circumferential effects of the test region could be neglected. Then by supplying air through the plenum, flow between the two test rings at a particular radius could be approximated by Poiseuille flow. This approximation could only be made for small intervals in the radial direction. In Poiseuille flow all derivatives in the direction of the flow are zero except the pressure term in the momentum equation, i.e., nothing changes with respect to the direction of flow. However, in the flow that was approximated as Poiseuille flow the velocity and the pressure does change in the direction of the flow, i.e., in the radial direction. But by taking small radial intervals and by making the gap width small, flow variables were considered constant and thus approximated Poiseuille flow. Therefore, the probe was calibrated in the test rig. In Poiseuille flow[11] the wall shear stress is given by:

$$\tau_w = - \frac{1}{2} (g) \frac{dP}{dr} \quad . \tag{31}$$

The radial pressure distribution term in the above expression was approximated by recording the pressure difference between two pressure taps, radially separated by the surface probe. The pressure taps were

not located in the same general area of the probe. This was possible because of the assumed axisymmetry of the flow. The expression for the shear stress (Equation 31) is also based on the assumption of the flow being fully developed. Yet, if one assumes that the hydrodynamic entry length is approximated by:[11,12]

$$\frac{Re_Q}{20} = \frac{x}{D} \tag{32}$$

where the Re_Q is based on the gap, all of the probe's mounting positions were in the fully developed flow regime (Appendix D). So by measuring the flow rate and pressure gradient across the surface probe, one could then calculate the surface shear stress across the probe. Then by plotting the calculated shear stress against measured voltage a calibration curve was obtained. This procedure was done for various gap widths ranging between 0.010 to 0.020 inches and varying flow rates. All these points fell within experimental error, however, data taken at gaps widths of 0.010 inches or less had larger deviations from this curve. This deviation of calculated shear stresses from the curve at a gap of 0.010 of an inch was originally thought to be due to surface variations of the test section. However, this was found not to be the only reason and will be discussed later.

CHAPTER IV

EXPERIMENTAL PROCEDURES

Certain inspections and procedures dealing with equipment had to be carried out before any testing could be conducted. One instrument that required inspection after each time it had been repositioned was the surface probe. Since the hot film surface probe measurements heavily depended on direction, it was carefully aligned after it was mounted. The probe was also sensitive to the relative flushness between itself and the stator, therefore, this was inspected once per remounting. Once the probe had been inspected, other pieces of equipment could then be set. For instance, the gap was then set by recording the spacing between the two disks in eight different places. This was accomplished by using the micrometer mounted on the stator and turning the rotor in 45 degree increments and obtaining a gap reading at each interval. The gap setting was obtained by averaging the eight readings. The maximum variations of the reading were on the order of 0.0005 of an inch. (Because of small surface variations in both the rings on the rotor and stator plus the very small amount of misalignment of the two disks, the gap widths were set to within $\pm$0.0005 of an inch.) At this point, the oil level in the manometer was set to zero and the level of the manometer adjusted. The regulator between the building's air supply and the line connecting the air filter used in this experiment were then set at 50 psi. The monitor and

supply system was then connected to the probe and switched on. Each day the overheat resistance in the hot wire circuit was set according to the procedures in the Thermo-Systems Manual, after a 10 to 15 minute warm-up period. Following the setting of the overheat resistance, it was possible to set the desired volumetric air flow rate using the valves in the two Dwyer rotormeters. The test rig, after daily inspection and calibration procedures had been carried out, was ready to be used in collecting data.

The process of collecting data went as follows:

1) Inspection and calibration of test rig and support system.
2) Air flow and rotor speed set by valves and motor control respectively.
3) Recording of the pressure at nine different pressure taps.
4) Recording voltage output of the probe from the 1050 monitoring system.
5) Resetting gap width, volumetric flow rate of air, and/or motor speed.
6) Repeating steps 3 through 5 with the addition of rechecking the probe's overheat resistance.

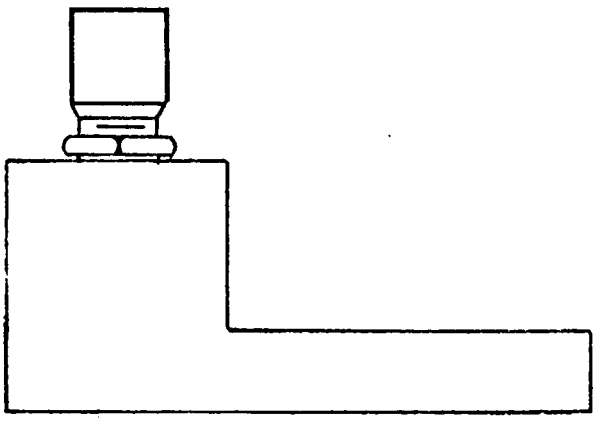
It should be noted that the variance of the speed was maintained to less than plus or minus 10 RPM of the desired rotational speed and the gap settings were considered to be set within 0.0010 of an inch, even though the gap settings were set closer.

CHAPTER V

THE THERMO-SYSTEM 1237W FLUSH SURFACE PROBE

A large part of this experiment dealt with obtaining surface shear stress data on the stator by the use of a Thermo-Systems 1237W Flush Surface Probe. A literature survey failed to yield any information concerning the directional characteristics of this flush sensor. Tests were conducted to determine the 1237W Flush Surface Probe dependence on direction and the effect of how positioning the probe sensing surface relative to the test surface affected the output signal of the probe.

To test the sensitivity of the probe to direction, a known one-dimensional shear stress had to be generated. Therefore, the flow that was used to approximate Poiseuille flow was an ideal choice. If the probe was heavily dependent on direction, by positioning the sensor 90 degrees out of phase the probe's signal should be greatly reduced. Four gap widths (0.010, 0.014, 0.016, 0.020 inches) and six volumetric flow rates (50, 100, 150, 200, 250, and 300 SCFH) were used in determining the directional dependence. The probe's mount (Figure 12) had lines inscribed radially about the center, 45 degrees apart. (In referring to these lines the line parallel to a radius will be called 0 degrees). Then the probe is also said to be mounted in the zero direction (Figure 12). Thus when the probe is at 90 degrees it is positioned to measure radial shear. Ninety, 45, and



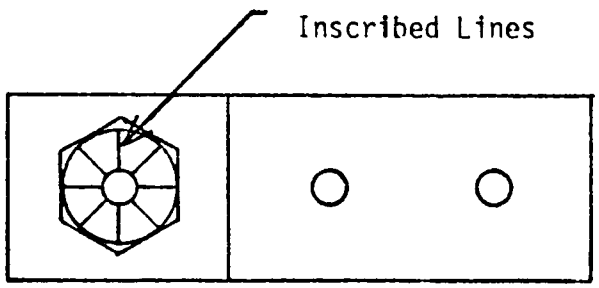


Figure 12. Probe Mount.

0 degrees were chosen as the angles to be studied. The voltage output of the probe was usually in the range of 13.0 to 13.7 volts, thus the percent of voltage output between two readings was given by:

$$\text{Error} = \left[\frac{V - 13.0}{Vo - 13}\right] \times 100 \qquad (32)$$

The voltage output at 0 degrees was an average of 81.4 percent of the 90 degree position, while the 45 degree position was 92 percent of the 90 degree position. The probe did show a slight directional dependence, but not, however, as much as a hot wire anamometer (Appendix G.3B). It should be noted that the probe mount was not designed for the sensor to rotate in and maintain the relative flushness, and therefore, this may have influenced these results. Also this mount was not designed to measure the probe's depth, therefore the discussion of the influence of the probe mounting, relative to being flush with the test surface, will be qualitative in nature. Pushing or pulling the probe from the back side of the stator, thus changing the depth the probe protruded or was reset back into the aluminum, while still maintaining the sensor "close" to the stator test section surface, could change the voltage output by $\pm$0.10 volts. This amounted to a total output voltage change of less than 1 percent. However, since all the reading ranged from 13.1 volts to 13.6 volts, this represents a larger error than 2 percent. In fact, a 0.01 volt represents 20 percent of the range of voltage measured.

The Thermo Systems 1237W Flush Probe was also sensitive to the conditions of incoming air.* For example, as the data was taken during the day, starting in the morning, the overheat resistance would change from about 5.67 to 5.73 ohms. It was concluded that as the ambient air's temperature warmed up during the day, the overheat resistance changed proportionally. To get good repeatability of data, runs had to be made at or close ($\pm$0.01 ohm) to the same overheat resistance.

---

*This condition was brought about after the building's air compressor broke down and air was supplied by the Department of Mechanical and Aerospace Engineering compressor.

CHAPTER VI

ANALYTICAL AND EXPERIMENTAL RESULTS

A. General

The experimental findings on pressure distributions, shear stress profiles and necessary conditions for zero pressure differences between the plenum and ambient condition are presented graphically. Since the data were divided into the above-mentioned categories, the results were also presented in the same groups.

B. Pressure

One of the main goals of this investigation was to obtain pressure data. The range of pressure differences between the plenum and ambient conditions ranged from a positive 3 inches of water to a negative of 1.5 inches of water. The data obtained and analysis presented showed various influences on pressure due to changes in three physical parameters (gap width, air flow rate, and rotor speed).

Increasing the ingested air flow to the test rig always was associated with a positive increase in the pressure difference (i.e., pressure difference between the plenum and ambient conditions). This was not a linear relationship, in other words increasing the air flow rate from 50 to 200 SCFH would not increase the pressure difference by a factor of four (Figure 13). This would be especially true if the conditions were such that a flow rate of 50 SCFH located the pressure difference in the negative regime (vacuum) and a flow rate

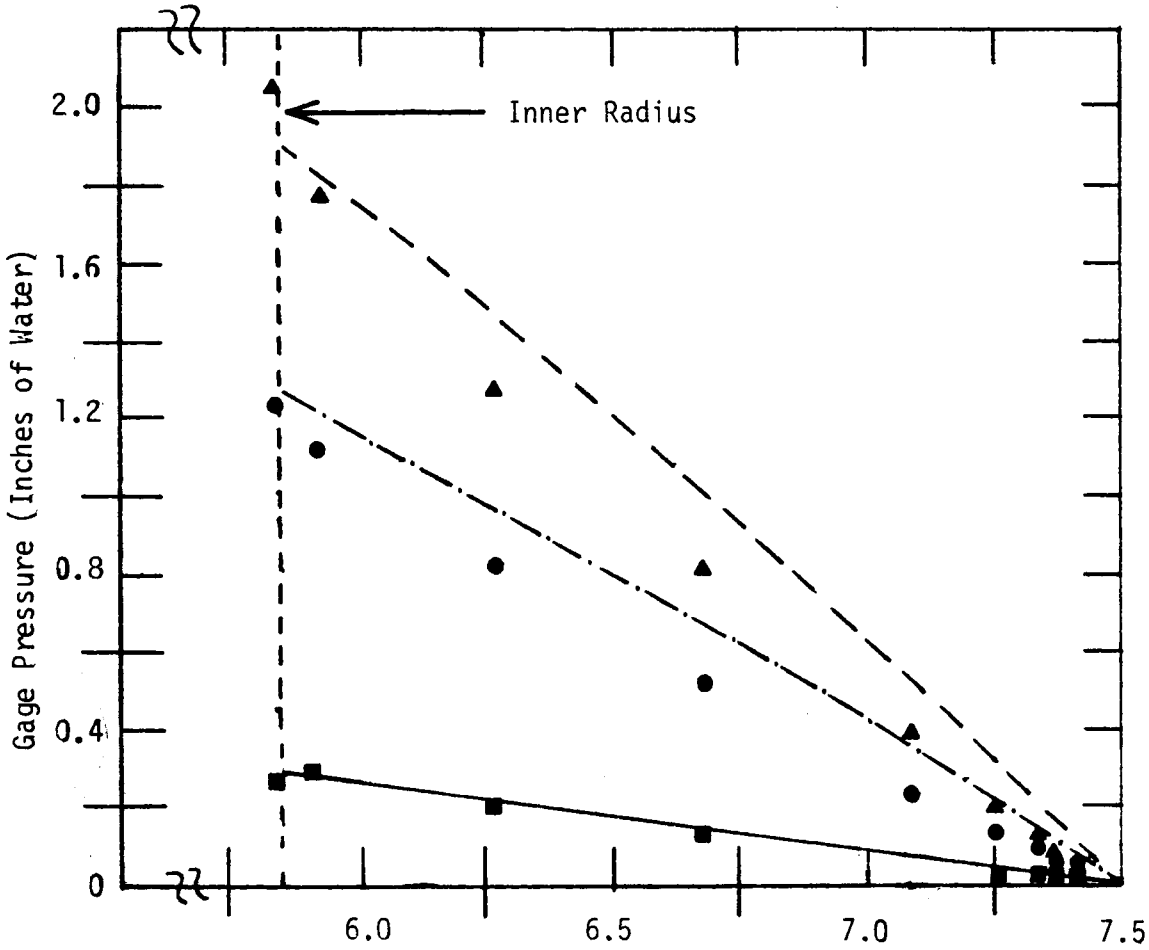
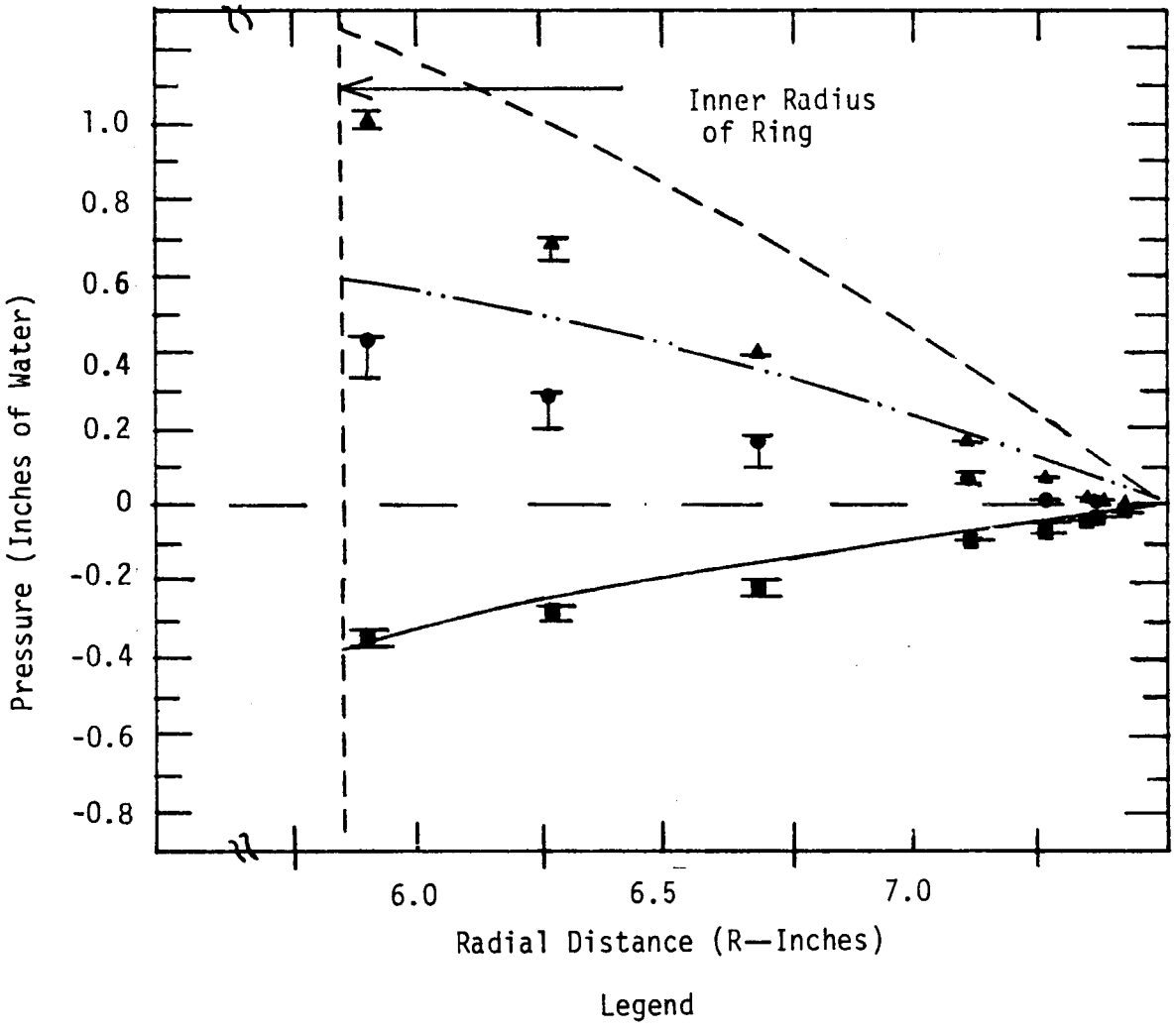


Figure 13. Comparison of Measured and Analytically Predicted Pressure Distributions I.

of 200 SCFH located the pressure in a positive regime (i.e., the pressure in the plenum was greater than the ambient condition) (Figure 14). The quadratic analysis was able to predict positive and vacuum pressure differences (Figures 13 and 14). For gaps less than 0.016 of an inch ($Rr < \frac{1}{468}$) the analysis predicted vacuum pressures within 0.02 inches of water of experimental data. Since the least count on the inclined manometer was $\pm$0.01 inches of water, pressure predictions for pressure less than this amount were considered correct if the data fell within this least count. A flow regime where the predictions failed to predict the correct pressure differences between the plenum and ambient conditions was for small gaps ($g \leq 0.010$ inches or $Rr \leq \frac{1}{750}$) and for pressure difference of 1.5 inches of water and higher. To obtain these pressures, flow rates of 200 and 300 SCFH had to be used at this width. This result, the failure of the analysis to predict these pressures, was not surprising since the radial velocity (U_o) became equal to or the same order-of-magnitude as the tangential (V_o). (Recall $\frac{U_o}{V_o} << 1$ was a basic assumption to the analysis.) In general, the analysis did a good job of predicting the pressure distribution when it predicted the correct pressure difference (Figure 14). There were cases, however, where the analysis predicted the correct pressure difference but failed to predict the correct pressure gradient (Figure 15). Generally this type of error occurred when the difference between the plenum and ambient conditions approached zero or when large pressure differences existed between the plenum and ambient conditions (1.50 to 1.70 inches of water or higher).

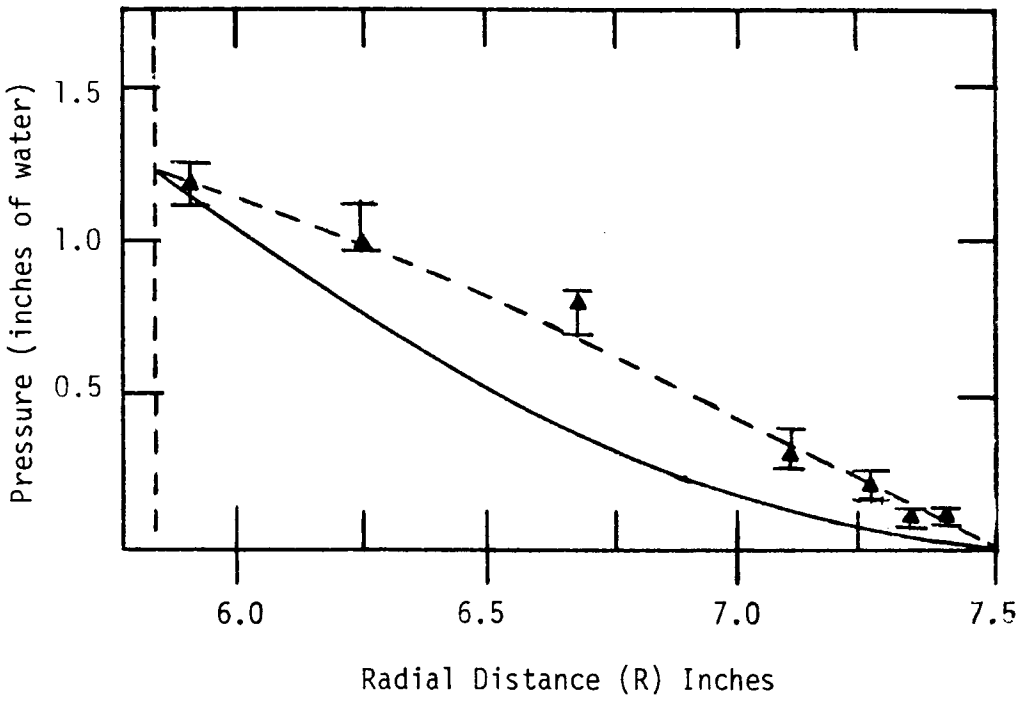


Legend

Quadratic Analysis	Data Point	SCFH
———	■	50
—— . .	●	200
— —	▲	300

($\dot{\theta}$ = 2500 RPM, Gap = 0.014")

Figure 14. Comparison of Measured and Analytically Predicted Pressure Distributions II.



Curve

Experimental Data ▲

Quadratic Analysis ————————

{$\dot{\theta}$ = 500 RPM, Gap = 0.014", Q = 200 SCFH}

Figure 15. Analytical Prediction of Pressure Profile.

The rotor's speed had just the opposite effect on pressure differences than did the air flow rate. For example, for a gap of 0.010 inches and flow rate of 50 SCFH, changing the rotor speed from 500 to 2000 RPM would change the pressure difference from 0.76 to 0.30 inches of water (Figure 16). The analysis accounted for this effect. Taking a condition that gives a negative pressure difference (vacuum) and increasing the rotor speed would result in a greater vacuum. In other words, increasing the rotor speed would cause an increase of pumping action. This additional pumping action, due to an increase in rotor speed, always decreased the pressure in the plenum (Figure 17).

The gap setting and rotor speed caused the pressure to respond similarly. Decreasing the gap setting would cause the pressure gradient across the test section (ring) to increase. The pressure increased exponentially with decreasing gap (Figure 18). Conditions where the pressure gradients across the ring exceeded 2.00 inches of water or higher had prediction errors in excess of 45 percent. To obtain these large pressures in the plenum required a large volumetric air flow rate and/or small gaps. Even though the gap ratio was small ($Rr = \frac{1}{750}$) a basic assumption to the analysis, the large flow rates associated with the small gap made the radial velocity (U_o) the same order of magnitude as the velocity in the tangential direction (V_o). Thus the basic assumption of $\frac{U_o}{V_o} << 1$ was not satisfied. Many non-dimensional groups and combinations of groups were examined, but the combination of Re, Pv and Rr (radial Reynolds number, the reciprocal of the tangential Reynolds number, and gap ratio respectively) formed in the following relationship:

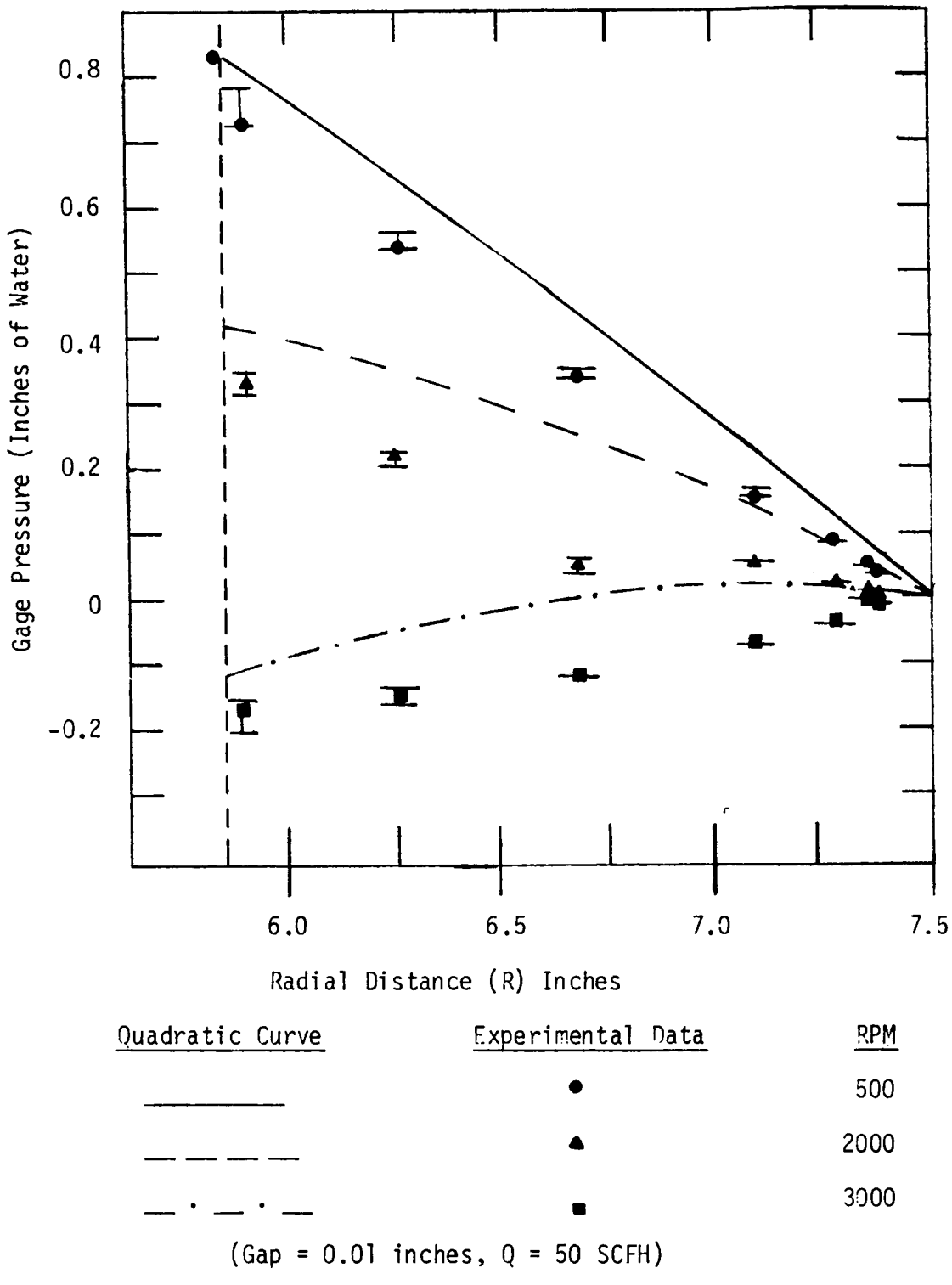


Figure 16. Comparison of Radial Pressure Distribution with Experimental Data.

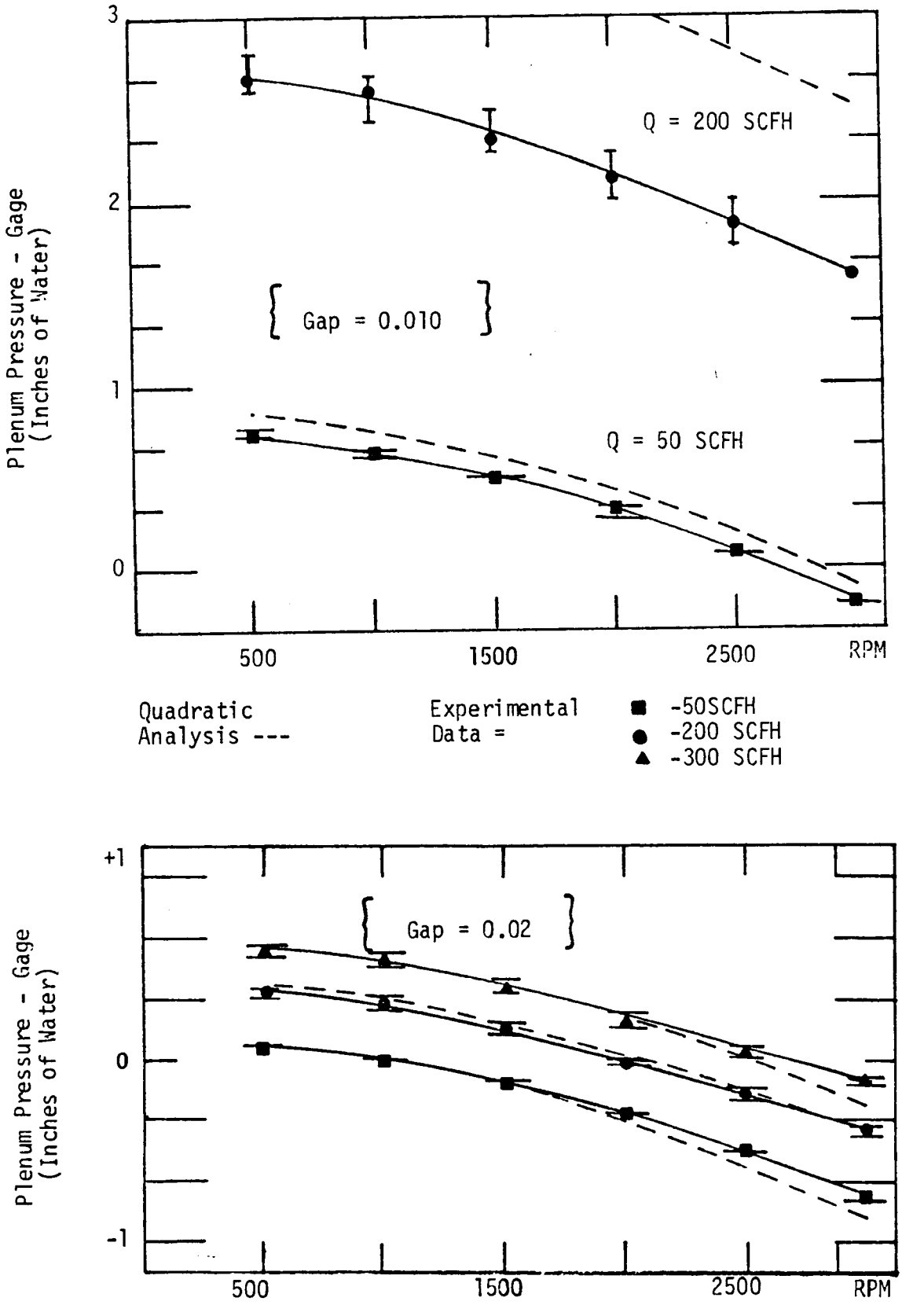


Figure 17. The Influence of Rotational Speed on Pressure.

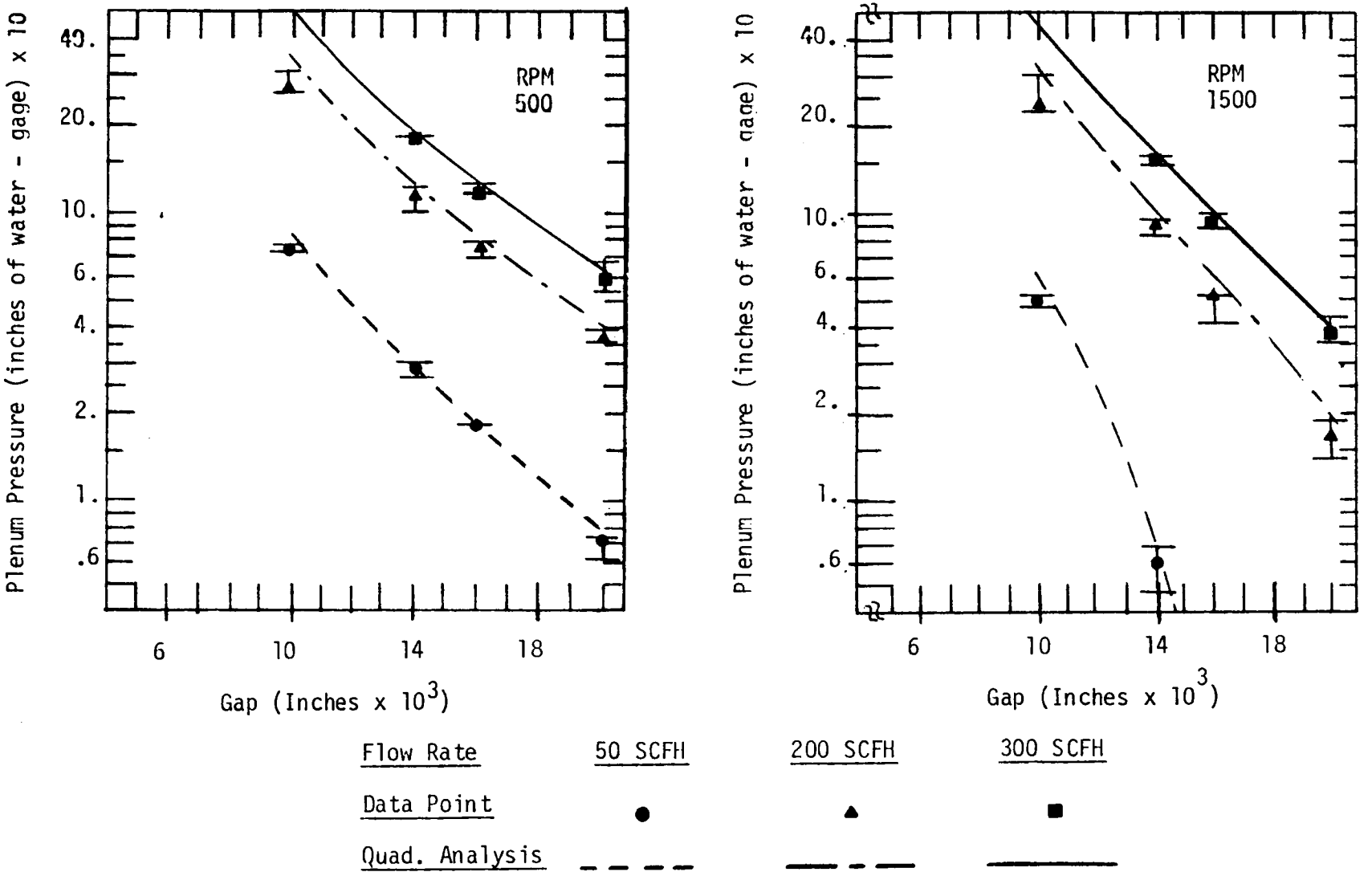


Figure 18. The Influence of Gap on Pressure.

$$\frac{Re}{Pv \; X \; Rr} \leq 38 \; (10)^9, \qquad (33)$$

best predicted where the analytic results applied. Dimensionally the above relation is a product of the Radial and Tangential Reynolds number divided by the radius ratio. Physically the above ratio is the product of the radial and tangential inertia forces divided by the product of the radial and tangential viscous forces, that ratio divided by the ratio of characteristic lengths (radius ratio - Rr = g/R_o).

Comparing the profiles predicted by the quadratic assumption and the predicted profiles of Pelech and Shapiro shows that the quadratic assumption made only second order corrections to the couette assumption. An example where the two analyses predicted essentially the same pressure gradient was for a gap of 0.01 inches, an air flow rate of 200 SCFH, and a rotor's speed of 500 RPM. Differences in the analyses tended to increase with rotor speed and gap width, while the difference between the two predictions tended to decrease with volumetric flow. Figure 19 shows a case where the quadratic and couette coincided. However, Figure 20 shows a situation where the quadratic assumption made second order corrections to the couette predictions.

Both analytically and experimentally the pressure was found to be a function of several parameters. The major parameter in determining the pressure in the plenum seemed to be the radial velocity. Experimentally the pressure difference was proportional to the flow rate and inversely proportional to the gap cubed. The analysis showed this as a ratio. That ratio is given by:

$$P \simeq \frac{Q}{g^3} \qquad (34)$$

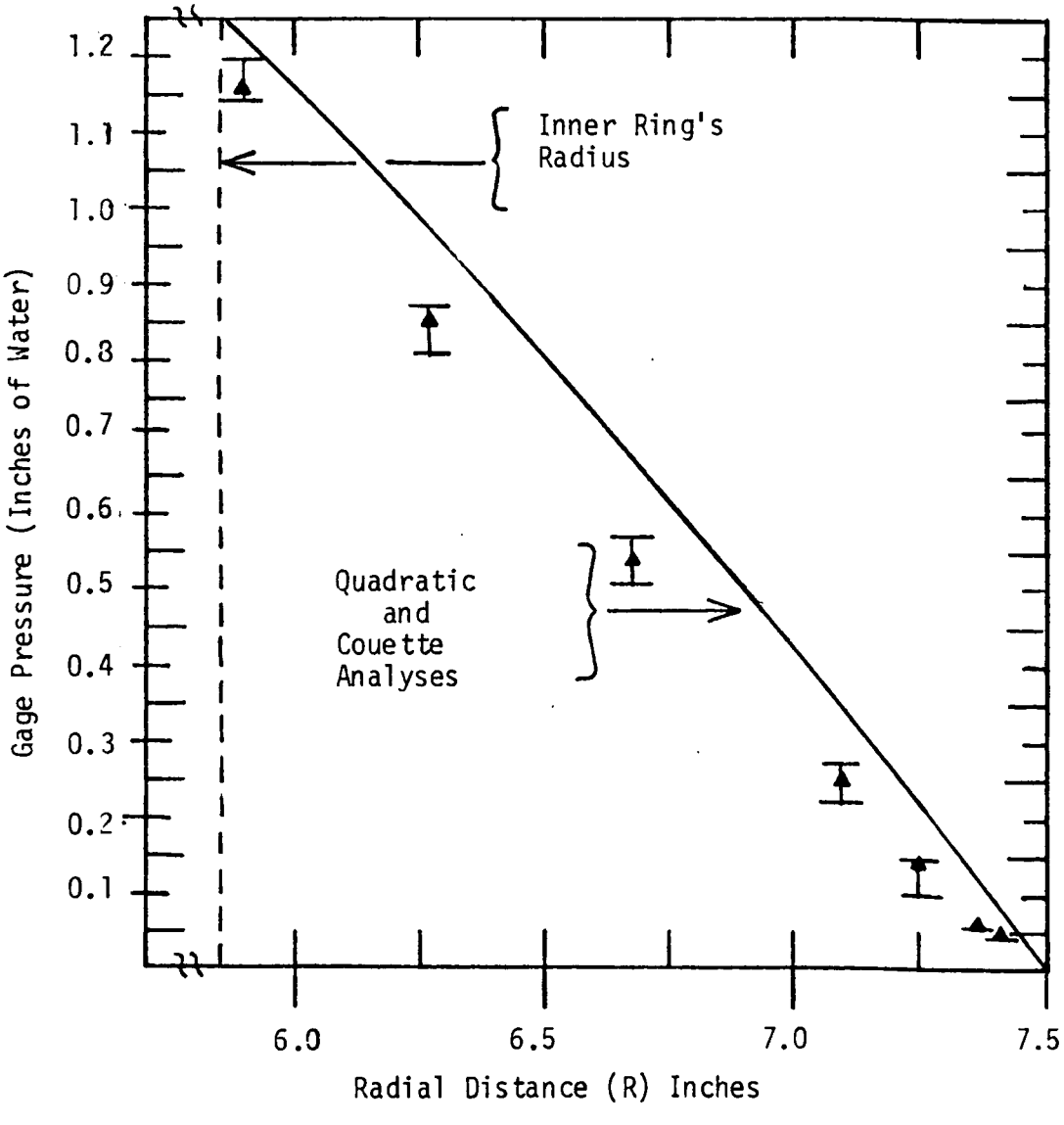


Figure 19. Comparison of the Analytical Prediction of Pressure with Experimental Data I.

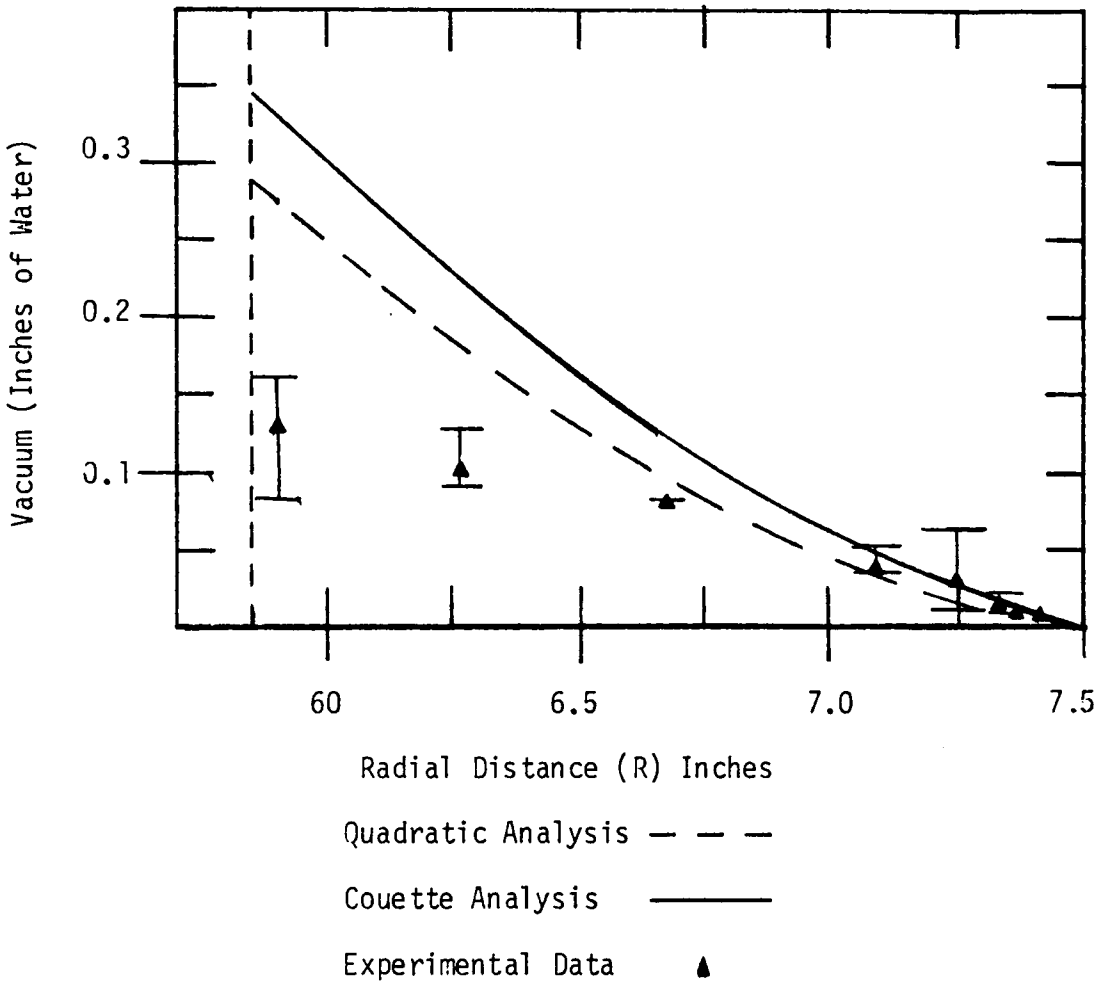


Figure 20. Comparison of the Analytical Prediction of Pressure with Experimental Data II.

This proportionality just shows the influence that two parameters, Q, the volumetric flow rate, and g, the gap setting, have on the pressure difference between the plenum and ambient conditions. The pressure also had an influence from the rotor's speed. By increasing the speed the pressure would decrease in the plenum. Again the analysis showed this in the form:

$$P \sim - \dot{\theta}^2 r^2 \tag{34}$$

In other words the plenum pressure decreased in proportion to the square of the rotor's speed. The analysis combined these two effects which can be shown by the following equation:

$$P \sim \frac{Q}{S3} - \dot{\theta}^2 r^2 \tag{35}$$

The above expression is only presented to give insight to what small perturbations of physical parameters would have on the pressure gradient across the test ring. (These influences are shown experimentally and the trends are also predicted analytically.)

One last note on the pressure predictions. Although the analysis had regions of errors, sometimes in excess of 50 percent, the predictions always fell within the uncertainty of the data (Appendix D).

C. Surface Shear Stress

The shear stress was also affected by the same three variables as the pressure, namely, the rotor speed, the spacing of the disks, and the ingested flow rate of air. The surface shear stresses seem to have two different regimes. These regimes usually were separated by a plenum gage pressure of zero. The shear stress characteristic response was different in a positive pressure field than in a negative pressure field.

Fixing the rotor's speed and air flow rate, the tangential shear stress would be reduced by doubling the gap, but not necessarily by a factor of two. The analysis did predict this halving trend. But in this case the shear stress depended upon other factors, such as the volumetric air flow. For example, maintaining the rotor's speed at 1000 RPM for three flow rates (50, 200, and 300 SCFH) of air while changing the gap setting from 0.020 inches to 0.010 inches will increase the shear stresses by factors of 1.55, 1.90, and 2.53, respectively (Figure 21). Varying the flow rate of air, which was injected into the disk pack, could change and have a big effect on the shear stress measurements. A reasonable hypothesis about the tangential surface shear stress on the stator would be, that it should increase with volumetric flow rate. However, this was not necessarily so. This depended on where the flow regime was (a positive, negative, or a zero pressure difference between the plenum and ambient conditions). The shear stress on the stator was dependent on the existing pressure difference across the test section. Increasing the flow rate of air from a positive pressure field would always result in an increase of the shear stress on the stator. Changing the pressure in the plenum from a vacuum, i.e. less than ambient, to zero pressure difference by increasing the air flow rate would cause the tangential shear stresses to decrease on the stator. Then increasing the flow rate past zero pressure difference would cause the shear stresses to increase. Thus, in all measurements for a given gap and rotor speed the minimum shear stress occurred at or very near zero pressure difference between the plenum and ambient conditions. Increasing the air flow rate from this

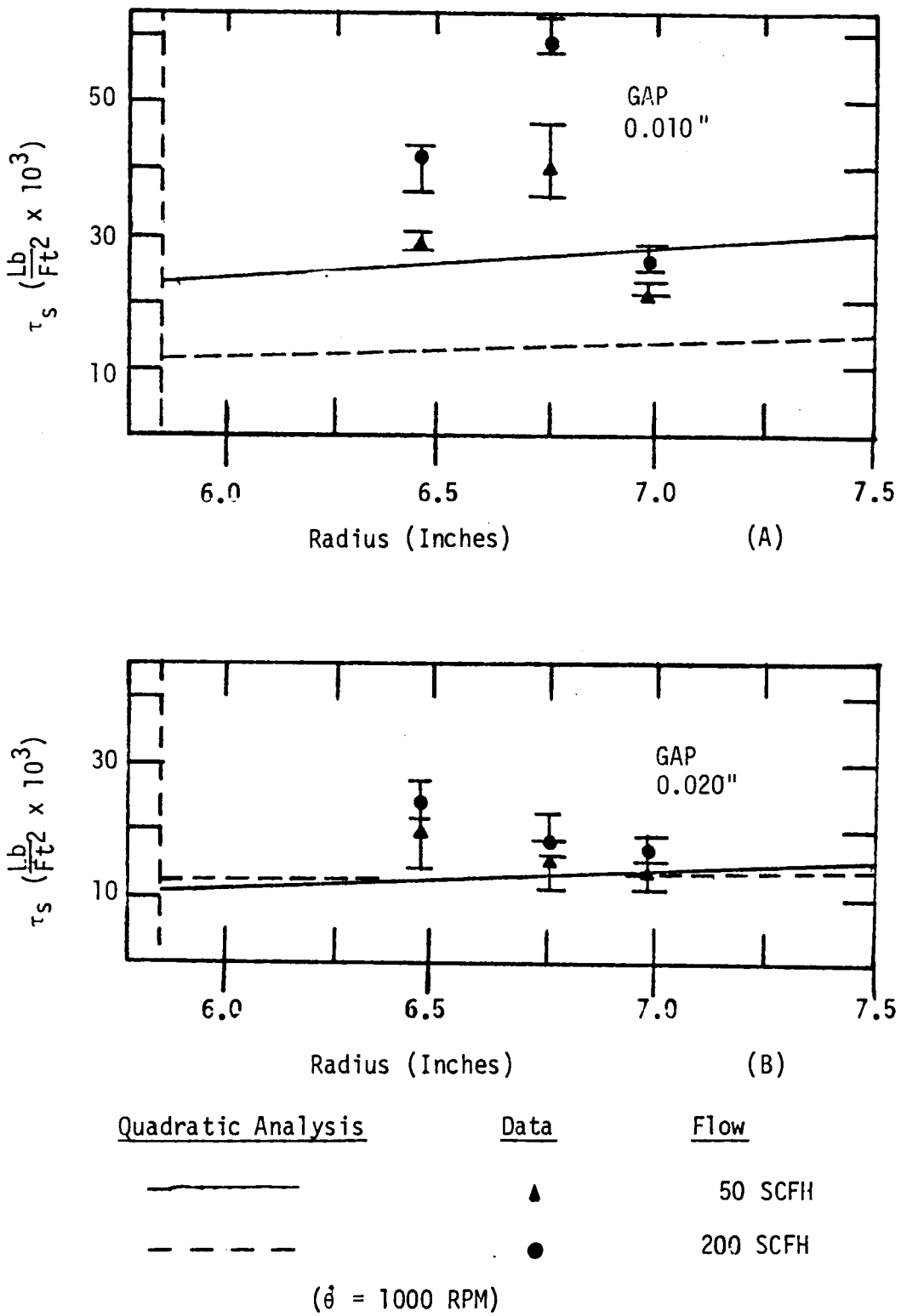


Figure 21. Comparison of Experimental Data for Shear Stress Distribution with Analytical Prediction.

condition would result in an increase in the shear stress experienced by the stator (Figure 22). Both analyses predicted that the shear stress would decrease when the air flow rate was increased. They predicted shear stresses as they responded in the vacuum pressure regime. This points out the fact that neither the quadratic analysis nor the analysis done by Pelech and Shapiro could predict the two regimes for the surface shear stress (Figure 22).

The rotor speed had a more direct influence upon the shear stress on the stator than did the volumetric air flow rate. Increasing the rotor speed while maintaining the gap and air flow rate constant would always result in an increase in the tangential shear stress. This was the case for all pressure gradients. Both analyses predicted a doubling of the tangential shear stresses on the stator by doubling the speed. However, this was not the case for most of the data taken. In fact, there was no constant ratio obtained in the increase of shear stress by doubling the rotor's speed.

In this investigation only three positions were available for shear measurements. These measurements seem to point out that the shear stress on the stator reaches a maximum in the center of the test section (i.e., $r = 6.69$ inches, or $\bar{R} = 0.89$) for positive pressures. However, for vacuum, the general trend was for the shear stress to decrease montonically with radius. The only exception to this was found at a gap of 0.014 inches. The couette and quadratic analyses failed to predict maximum in the surface shear stress distribution. In fact, the analyses predicted a shear stress distribution that increased montonically with increasing radius (Figure 23).

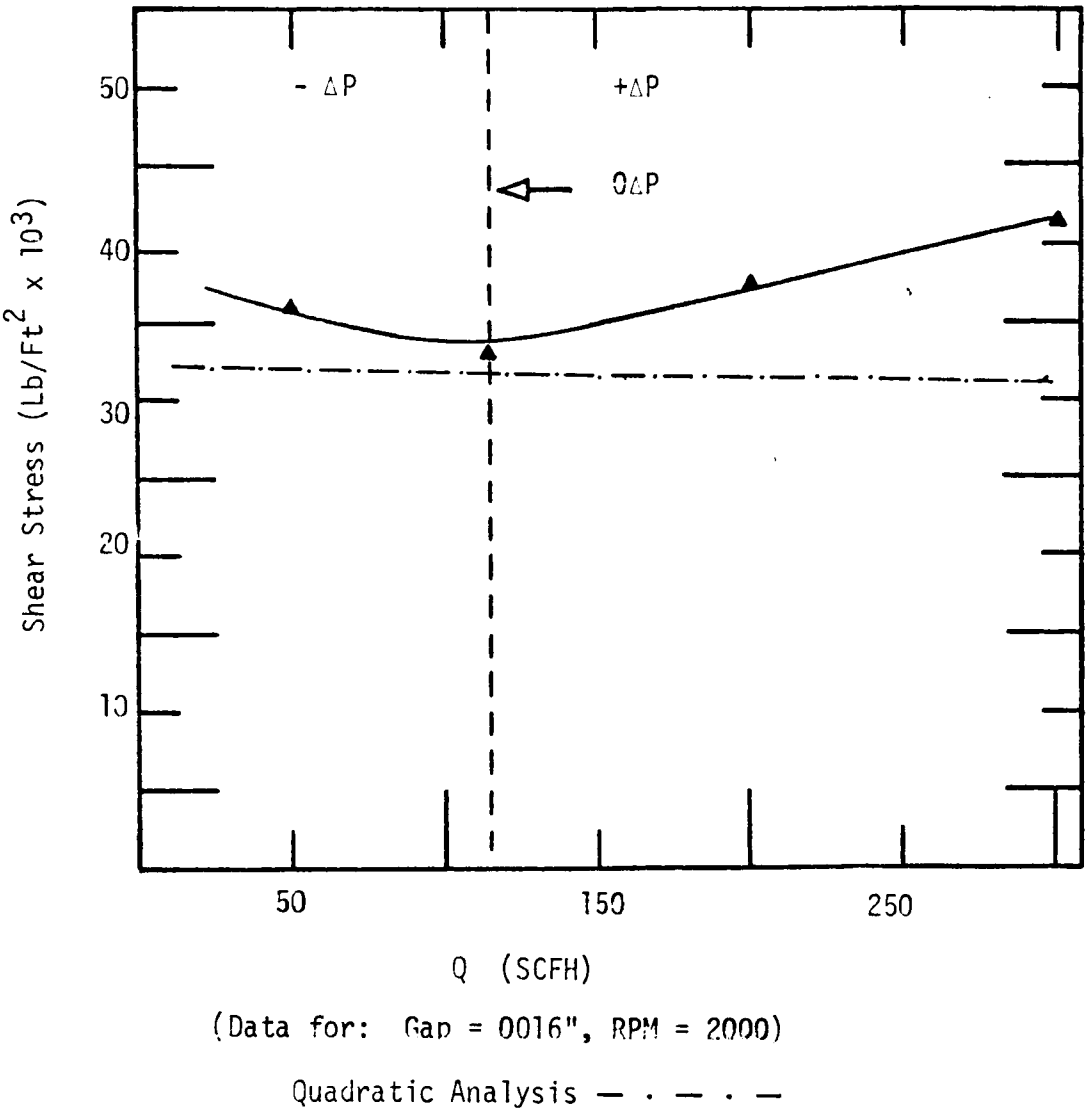


Figure 22. Comparison of Average Shear Stress to the Analytical Predicted Average.

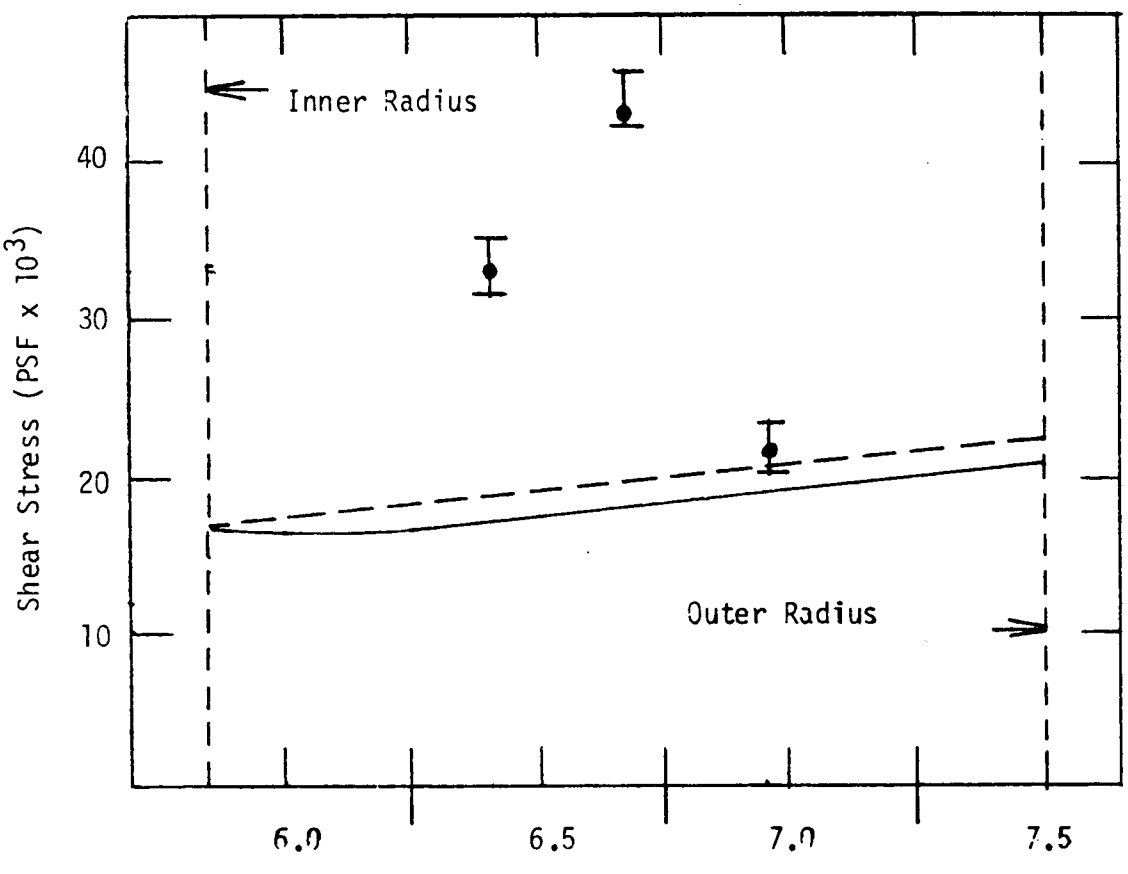


Figure 23. Comparison of Analytical Predicted Shear Stress Profile with Experimental Data.

D. Zero Pressure Difference

Since zero pressure difference has been shown to minimize the drag on the stator, it was imperative to predict the required flow rate of fluid (air) that would give this condition. Both analyses, the quadratic and the couette, predicted the flow rates required to accomplish this task (Figure 24). It should be noted that the quadratic analysis made second order correction to the predictions made by the couette assumption. For example, the couette assumption predicted a flow rate of 456 SCFH for a gap of 0.020 inches and a rotor speed of 3000 RPM, while the quadratic predicted a flow rate of 424 SCFH. In this case, the only flow condition studied that both analyses failed to predict the flow rate within the experimental range of data, was 360 SCFH. Because the quadratic analysis was only a few percent better than the couette analysis, and since the couette equation giving the required flow rate of fluid for zero pressure difference was in a simple closed algebraic form, and the same equation for the flow rate developed from the quadratic assumption required numerical techniques to solve, the couette equation will be presented. This equation was given by:

$$\Delta P = 0 = \rho\dot{\theta}^2(r_1^2 - r_0^2)\frac{3}{20} - \frac{6Q\mu}{\pi S^3}\ln\left(\frac{r_1}{r_0}\right) \qquad (36)$$

Equation (36) was arrived at by integrating equation (6) with respect to the radial coordinate. Equation (36) successfully predicted the flow rate for all gaps tested (gaps 0.010 - 0.020 inches or Rr from $\frac{1}{750} - \frac{1}{375}$).

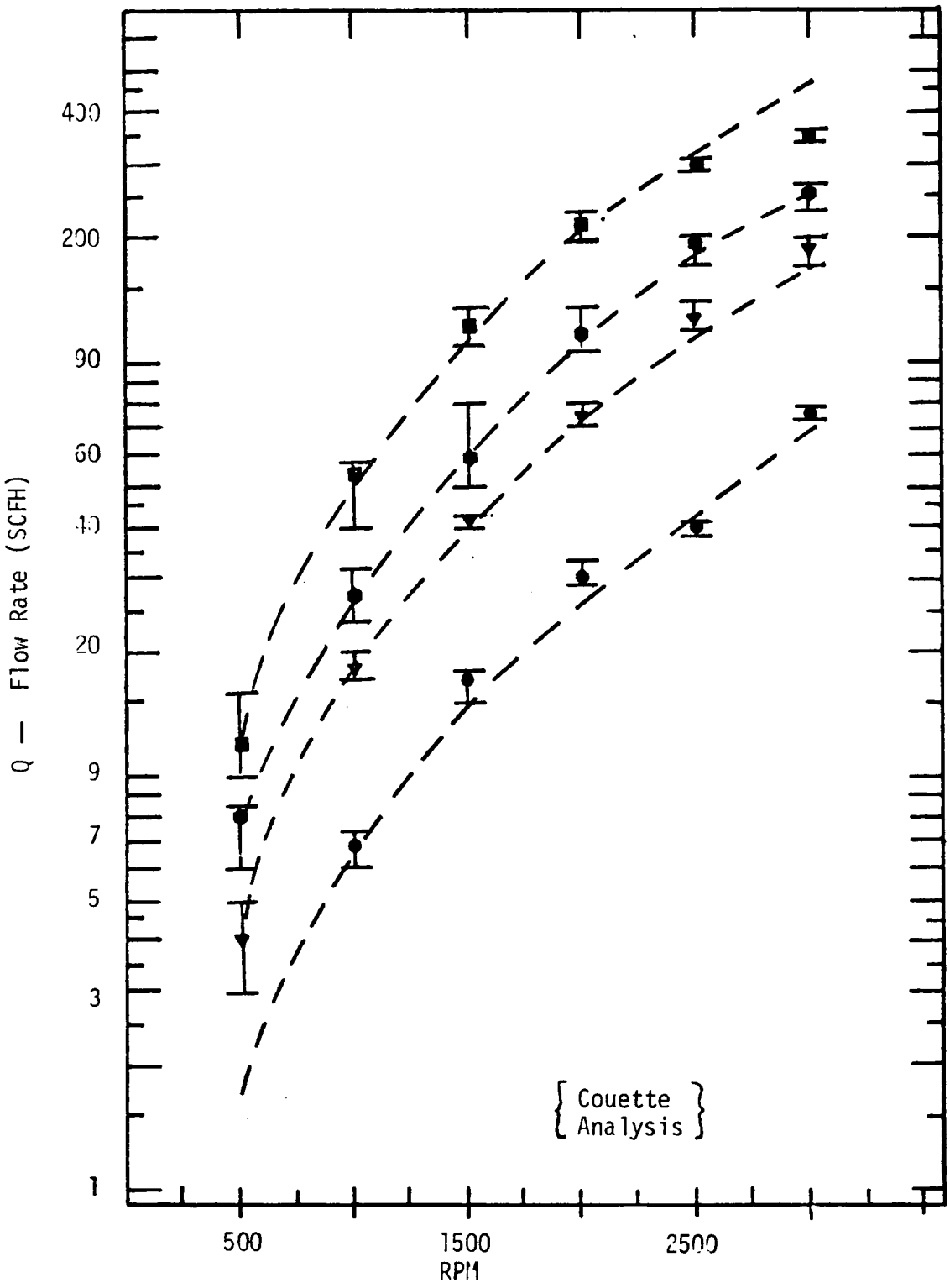


Figure 24. Comparison of Analytically Predicted Flow Rate for Zero Pressure Difference with Experimental Data.

E. Assumption of Axisymmetry

As was previously stated, there were two pressure taps in the test section of the stator to check the assumption of axisymmetry (in particular $\frac{\partial P}{\partial \theta}$). The two taps located approximately 135 degrees apart at a radius of 6.265 inches ($\overline{R}$ = 0.84). One of the taps was placed directly on the bottom side of the disk (Figure 25). The Dwyer manometer was then connected in series between the two pressure taps. For a volumetric flow rate of 50 SCFH, no pressure difference was recorded for any gap and speed combination used in this investigation. But when a flow of 200 or 300 SCFH was tested there did exist a pressure differential. The biggest difference recorded was not more than 0.04 inches of water. This was due to the proximity of the table to the bottom tap location. However, it was believed that this was a local perturbation. It should be noted that none of the mounting holes for the flush surface probe or pressure taps used in data acquisition were located in this area.

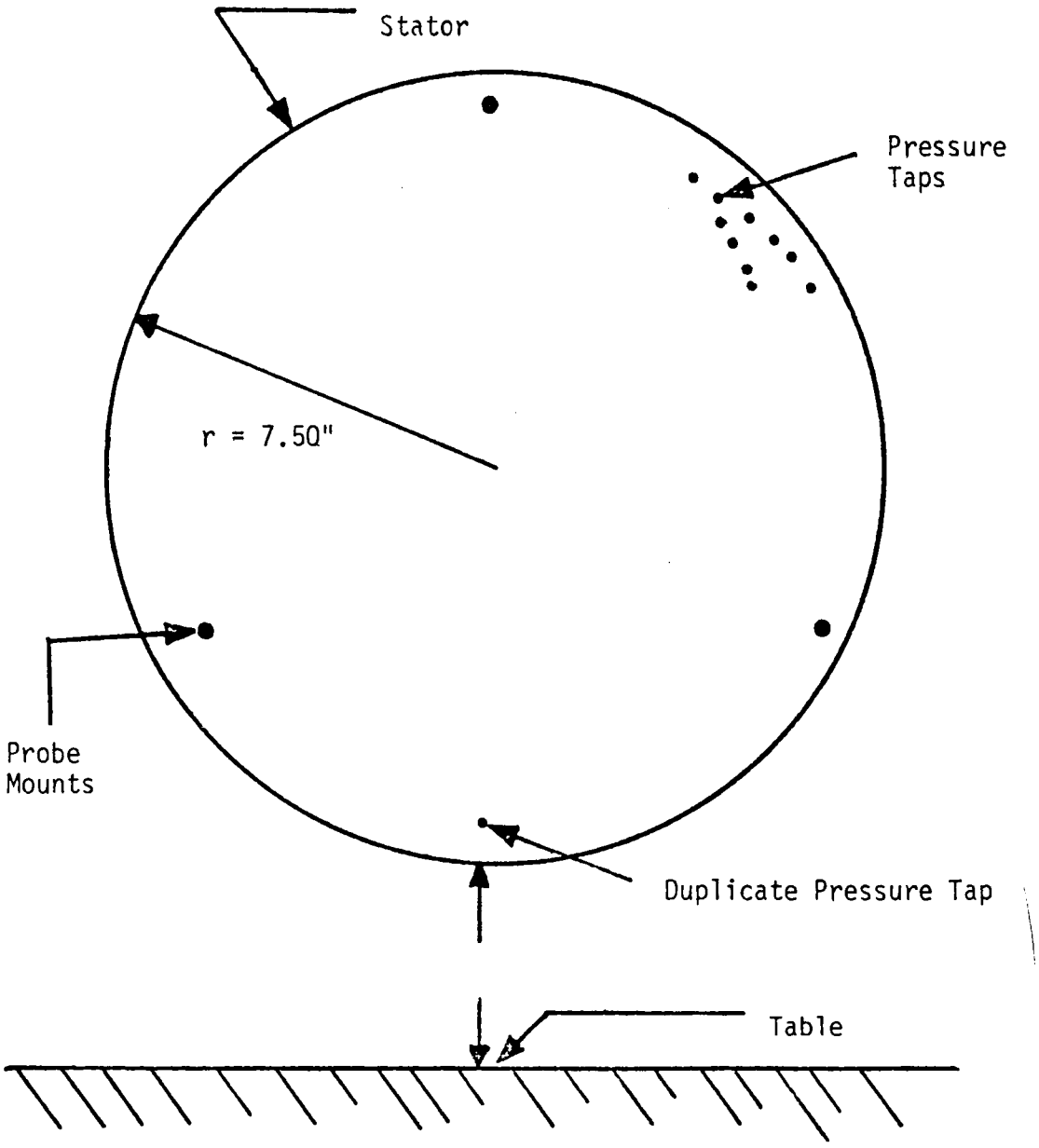


Figure 25. Relative Positions of Pressure Taps and Table.

CHAPTER VII

CONCLUSIONS

The pressure predictions made by both analyses, the couette and the quadratic tangential velocity profile, were in many instances within 1 percent of the data. In fact, the quadratic analysis made only second order corrections to the analysis employing the couette assumption. In the regime of $\frac{Re}{Pv * Rr} < 38\ (10)^9$ the analysis predicted the pressure difference within 20 percent or better. The quadratic analysis was more accurate at bigger gap widths (g = 0.020 inches or $Rr = \frac{1}{375}$) and at higher flow rates (200 SCFH or Pv > 1725). This is the only time that the quadratic profile should be used because of its added complexity. It was found, analytically and experimentally, that the pressure depended heavily on the radial flow. It was also found the pressure increased exponentially with decreasing gap as the gap approached 0.010 inches ($Rr = \frac{1}{750}$) from the larger setting.

The shear stress was influenced by a number of physical characteristics and flow regimes which the present analysis did not take into account. The data indicated that the condition for optimum operation, minimum drag, for a closely spaced rotor and stator is at zero pressure difference. Another item that the computer models did not predict was a peaking of tangential shear stress on the stator mid-way across the test section ($\overline{R} = 0.89$) for positive pressures. This could be caused by the sharp inlet to the test section from the plenum. For high flow rates of fluid (air), i.e. associated with

large pressure differences between the plenum and ambient conditions, separation might have occurred at the edge of the test section, thus causing a decrease in shear stress at the inner radius. The only exception to the shear stress trend of maximizing for positive pressure differences occurred at a gap of 0.014 inches. The shear stress showed a dip toward the center of the test section or in general decreased along a radius for vacuums or zero pressure differences.

Because zero pressure difference represents the minimum drag condition, an expression for predicting the flow rate required for a given speed, gap (radius ratio) was found by Pelech and Shapiro to be this expression:

$$0 = \rho\dot{\theta}^2 (r_1^2 - r_0^2) \frac{3}{20} - \frac{60\mu}{\pi g^3} \ln \left(\frac{r_1}{r_0}\right) \qquad (37)$$

This expression showed good results in predicting the volumetric flow rates of air (Figure 26). It should be noted why the equation developed by the couette analysis was given and discussed instead of the equation developed by the quadratic analysis. The equation, developed from the assumption of a quadratic velocity predicting the amount of volumetric flow, was not in a closed form and required numerical techniques to obtain answers. The same equation developed by assuming a couette profile for the tangential velocity distribution yielded a simple closed algebraic form, differing from the quadratic by only a few percent.

In general, the quadratic analysis only made second order corrections to the couette analysis for air. However, Figure 20 (p. 44) shows that the two analyses did have regions where there were differences in predictions. The difference between the two analyses was the

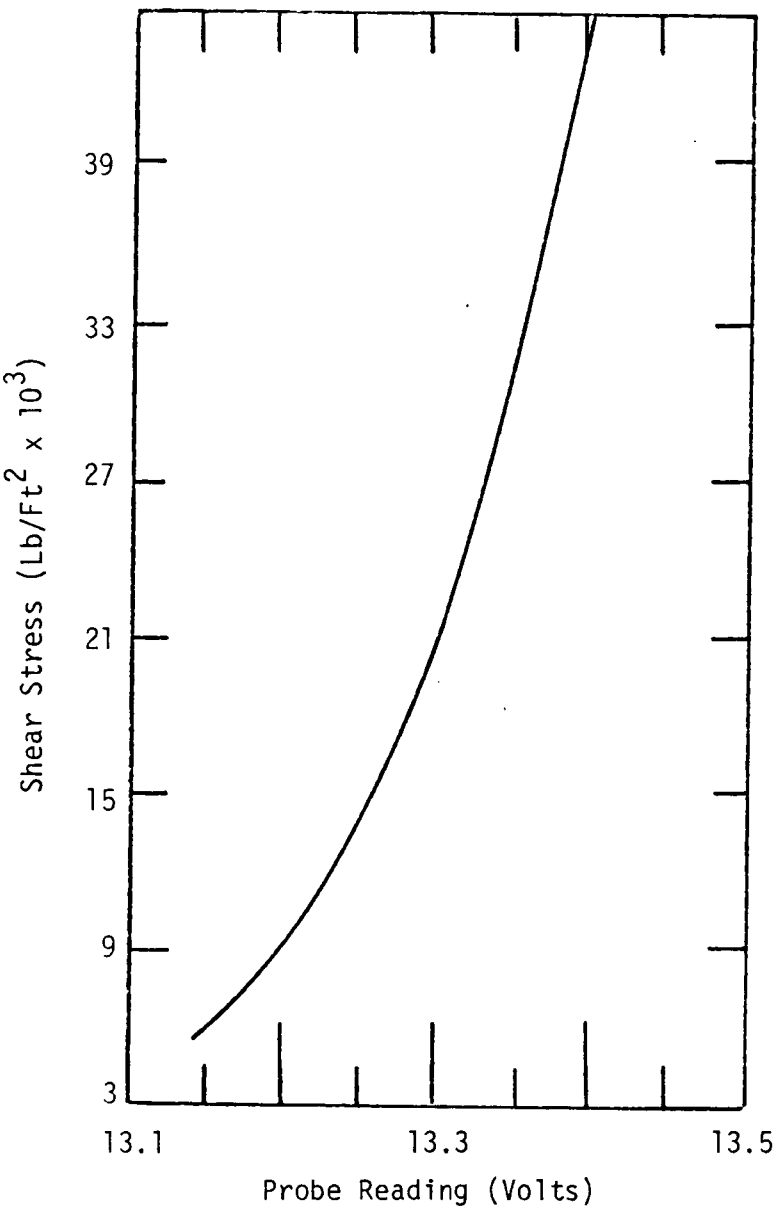


Figure 26. Hot Film Surface Probe Calibration Curve.

coefficient of the squared term in the tangential velocity distribution, C. Equation 20 gives the expression for C, and is listed below:

$$C = \frac{\dot{\theta}Q}{4\pi g\nu}\left(\frac{1}{r}\right)\left(1-\exp\left[\frac{12\pi\nu}{gQ}\left(r_1^2 - r^{21}\right)\right]\right) \qquad (20)$$

If SAE 10 weight oil had been used in this investigation instead of air, the difference between the two analyses, couette and quadratic, would have been more noticeable. This can be seen by noting that C is a function of the kinematic viscosity. SAE 10 weight oil has a kinematic viscosity 85 times that of air at 77 degrees F. There are fluids and flow regimes that the quadratic assumption might have a significant advantage in predicting the correct pressure differences and gradients over the couette analysis.

CHAPTER VIII

RECOMMENDATIONS

If further research is carried out in this field, and this test rig is used in the collection of more data, three items should be changed. The first item that should be changed is the addition of several additional mounting locations for the surface shear stress probe in the stator test section. This would help verify the shear stress profile on the stator. Secondly, the stator test section should be machined parallel to the back side of the stator. This would allow only one setting on the probe mount and thus increase reliability of readings while minimizing the effort involved in repositioning the probe. The scatter in the calibration curve of the shear probe could be reduced by the construction of a calibration rig. The design of this rig should pay special attention to improvements in setting gaps and supplying known and uniform flow rates of air. This would cut down the scatter at higher shear stress readings. A third modification that should be made to the rig has to deal with the axisymmetry assumption. The flow disturbance due to the proximity of the table could be corrected by either raising the disks or cutting a slot in the table to allow air to move freely about the disk. Although not very significant, this should be done to prevent circumferential pressure gradients.

Finally the pressure predictions and the predictions for air flow rates giving zero pressure difference should only be used in flow fields where the value of $\frac{Re}{PV * Rr}$ is less than $38 \times (10)^9$.

LIST OF REFERENCES

LIST OF REFERENCES

1. Missimer, J. R., "Analytical Model of Flow Between Smooth Stationary Disk and Grooved Rotating Disk," dissertation, Department of Mechanical and Aerospace Engineering, University of Tennessee, Knoxville, December 1979.

2. Bayley, F. J., and Owens, J. M., "Flow Between a Rotating and a Stationary Disk," Aeronautics Quarterly, 20, 33(1969).

3. Pelech, I., and Shapiro, A. H., "Flexible Disc Rotating on a Gas Film Next to a Wall," J. Applied Mech., pp. 577-584 (1964).

4. Szeri, G. W., and Adams, C. L., "Laminar Through Flow Between Closely Spaced Rotating Disks," J. Fluid Mechanics, vol. 86, Part 1, pp. 1-14.

5. De Nevers, N., Fluid Mechanics, Addison-Wesley (1970), p. 244.

6. Speckhart, F. H., and Green, W. L., A Guide to CSMP-The Continuous System Modeling Program, Prentice-Hall, 1976.

7. Bellhouse, B. J., and Schultz, D. L., "Determination of Mean and Dynamic Skin Friction, Separation and Transition in low-speed flow with a thin film heated element," J. Mech., vol. 24, part 2, pp. 349-400.

8. Blinco, P. H., and Simons, D. B., "Characteristics of Turbulent Boundary Shear Stress," Jour. of the Engineering Mechanics Division, ASCE, vol. 100, No. EM2, April 1974.

9. Blinco, P. H., and Simons, D. B., "Turbulent Structure Near Smooth Boundary," Jour. of the Engineering Mechanics Division, ASCE, vol. 101, No. EM3, June 1975.

10. Blinco, P. H., and Simons, D. B., "Measurement of Instantaneous Boundary Shear Stress," Pro. of the Hydraulic Division Specialty Conf., ASCE, Boseman, Montana, August 1973.

11. White, Frank M., Viscous Fluid Flow, McGraw Hill, 1974, p. 121.

12. Kays, W. M., Convection Heat and Mass Transfer, McGraw Hill, 1966. pp. 55 and 63.

13. Holman, J. P., Experimental Methods for Engineers, Sec. Edition. McGraw Hill, 1971, p. 37.

APPENDICES

APPENDIX A

DERIVATION OF GOVERNING EQUATIONS

This investigation studied the Steady State Laminar radial flow of a constant property Newtonian fluid between two parallel closely spaced rings mounted on two disks, one on a stationary disk, the other on a rotating disk.

The following list gives the assumptions made in the development of the analytical analysis.

1) Laminar Flow
2) Constant Property Newtonian Fluid
3) Steady State Flow ($\frac{\partial(\ )}{\partial +}$) = 0)
4) Axisymmetric Flow; this is due to the geometry of the flow
$$(\frac{\partial(\ )}{\partial \theta} = 0)$$
5) The characteristic length in the radial direction (the radius r_o) is much greater than the characteristic length in the axial direction (gap width = g) ($g/r_o << 1$).
6) The radial velocity (U_o) is much less than the tangential velocity (V_o) (i.e., $U_o/V_o << 1$).

Navier-Stokes Equations in Cylindrical Coordinates

Continuity:

$$\frac{1}{r}\ \frac{\partial}{\partial r}(rU) + \frac{1}{r}\frac{\partial V}{\partial \theta} + \frac{\partial W}{\partial Z} = 0$$

Radial Momentum:

$$\frac{\partial U}{\partial t} + U\frac{\partial U}{\partial r} + \frac{v}{r}\frac{\partial U}{\partial \theta} + W\frac{\partial U}{\partial Z} - \frac{v^2}{r} = -\frac{1}{\rho}\frac{\partial P}{\partial r} + F_r$$

$$+ \nu\left(\frac{1}{r}\frac{\partial}{\partial r}\left(r\frac{\partial U}{\partial r}\right) + \frac{1}{r^2}\frac{\partial^2 U}{\partial \theta^2} + \frac{\partial^2 U}{\partial Z^2} - \frac{U}{r^2} + \frac{2}{r^2}\frac{\partial v}{\partial \theta}\right)$$

Theta Momentum:

$$\frac{\partial W}{\partial t} + U\frac{\partial V}{\partial r} + \frac{v}{r}\frac{\partial v}{\partial \theta} + W\frac{\partial v}{\partial Z} + \frac{VU}{r} = \cdot\ \frac{-1}{\rho r}\frac{\partial P}{\partial \theta} + F_\theta$$

$$+ \nu\left(\frac{1}{r}\frac{\partial}{\partial r}\left(r\frac{\partial v}{\partial r}\right) + \frac{1}{r^2}\frac{\partial^2 v}{\partial \theta^2} + \frac{\partial^2 v}{\partial Z^2} + \frac{2}{r^2}\frac{\partial U}{\partial \theta} - \frac{v}{r^2}\right)$$

Axial Momentum:

$$\frac{\partial W}{\partial t} + U\frac{\partial W}{\partial r} + \frac{v}{r}\frac{\partial W}{\partial \theta} + W\frac{\partial W}{\partial Z} = -\frac{1}{\rho}\frac{\partial P}{\partial Z} + F_W$$

$$+ \nu\left(\frac{1}{r}\frac{\partial}{\partial r}\left(r\frac{\partial W}{\partial r}\right) + \frac{1}{r^2}\frac{\partial^2 W}{\partial \theta^2} + \frac{\partial^2 W}{\partial Z^2}\right)$$

Non-dimensional Variables

$$\overline{U} = \frac{U}{U_o} \qquad \overline{v} = \frac{v}{v_o} \qquad \overline{W} = \frac{W}{W_o} \qquad \overline{r} = \frac{r}{r_o} \quad (r_o = \text{outside radius})$$

$$\overline{Z} = \frac{Z}{Z_o} \quad (Z_o = \text{gap width}) \qquad \overline{P} = \frac{P}{P_o}$$

Non-dimensional Parameters

$$Re_v = \frac{V_o r_o}{r} \qquad Pv = \frac{r}{v_o Z_o} \qquad \theta = \frac{r_1}{r_o} \qquad Rr = \frac{g}{r_o}$$

To begin the analytical analysis, start reducing the continuity equation first.

Continuity:

$$\frac{1}{r}\frac{\partial}{\partial r}(ru) + \frac{1}{r}\frac{\partial v}{\partial \theta} + \frac{\partial W}{\partial Z} = 0$$

0

$$\frac{U_o}{r_o}\frac{1}{\bar{r}}\frac{\partial}{\partial \bar{r}}(\bar{r}\,\bar{U}) + \frac{W_o}{Z_o}\frac{\partial \bar{W}}{\partial \bar{Z}} = 0$$

Each term has to be $\theta(1)$

$$\frac{1}{\bar{r}}\frac{\partial(\bar{r}\bar{U})}{\partial \bar{r}} + \frac{W_o r_o}{Z_o U_o}\frac{\partial \bar{W}}{\partial \bar{Z}} = 0$$

Therefore,

$$\frac{W_o r_o}{Z_o U_o} = 1$$

This reduces the Non-dimensional Continuity Equation to

$$\frac{1}{\bar{r}}\frac{\partial(\bar{r}\bar{U})}{\partial \bar{r}} + \frac{\partial \bar{W}}{\partial \bar{Z}} = 0$$

Continuing on to the Radial Momentum Equation

$$\frac{\partial U}{\partial t} + U\frac{\partial U}{\partial r} + \frac{v}{r}\frac{\partial U}{\partial \theta} + W\frac{\partial U}{\partial r} - \frac{v^2}{r} = \frac{-1}{\rho}\frac{\partial P}{\partial r} + F_r$$

$0 = \frac{\partial}{\partial t}$ $\quad 0 = \frac{\partial}{\partial \theta}$ no body forces

$$+ \nu\left(\frac{1}{r}\frac{\partial}{\partial r}\left(r\frac{\partial U}{\partial r}\right) + \frac{1}{r^2}\frac{\partial^2 U}{\partial \theta^2} + \frac{\partial^2 U}{\partial Z^2} - \frac{U}{r^2} - \frac{\partial}{r^2}\frac{\partial v}{\partial \theta}\right.$$

$0 = \frac{\partial}{\partial \theta}$ $\quad 0 = \frac{\partial}{\partial \theta}$

$$U\frac{\partial U}{\partial r} + W\frac{\partial U}{\partial Z} - \frac{v^2}{r} = -\frac{1}{\rho}\frac{\partial P}{\partial r} + r\left[\frac{1}{r}\frac{\partial}{\partial r}\left(r\frac{\partial U}{\partial r}\right) + \frac{\partial^2 U}{\partial Z^2} - \frac{U}{r^2}\right]$$

Non-dimensionalizing the above equation,

$$\left(\frac{U_o^2}{r_o}\right)\bar{U}\frac{\partial \bar{U}}{\partial F} + \left(\frac{W_o U_o}{Z_o}\right)\bar{W}\frac{\partial \bar{U}}{\partial \bar{Z}} - \frac{V_o^2}{r_o}\frac{\bar{v}^2}{\bar{r}} = \frac{-P_o}{\rho r_o}\frac{\partial \bar{P}}{\partial \bar{r}}$$

$$+r\left[\frac{U_o}{r_o^2}\frac{1}{\bar{r}}\frac{\partial}{\partial F}\left(\bar{r}\frac{\partial \bar{U}}{\partial F}\right) + \frac{V_o}{Z_o^2}\frac{\partial^2 \bar{U}}{\partial \bar{Z}^2} - \frac{U_o}{r^2}\frac{\bar{U}}{F^2}\right]$$

divided by V_o^2/r_o

$$\left(\frac{U_o}{V_o}\right)^2 \frac{r_o}{r_o}\,\bar{U}\,\frac{\partial \bar{U}}{\partial \bar{F}} + \left(\frac{W_o U_o}{V_o^2}\,\frac{r_o}{Z_o}\right)\bar{W}\,\frac{\partial \bar{U}}{\partial \bar{Z}} - \frac{v^2}{r} = -\frac{1}{\rho}\left(\frac{P_o}{r_o}\,\frac{r_o}{V_o^2}\right)\frac{\partial \bar{P}}{\partial \bar{F}}$$

$$+ \nu\left(\left(\frac{U_o}{r_o}\,\frac{r_o}{V_o}\right)\frac{1}{F}\,\frac{\partial}{\partial \bar{r}}\left(\bar{r}\,\frac{\bar{U}}{\bar{r}}\right) + \frac{U_o}{Z_o^2}\,\frac{r_o}{V_o^2}\,\frac{\partial^2 \bar{U}}{\partial \bar{Z}^2} - \frac{U_o}{r^2}\,\frac{r_o}{V_o^2}\,\frac{U}{\bar{r}^2}\right)$$

recall $\frac{U_o}{V_o} << 1 \Rightarrow \left(\frac{U_o}{V_o}\right) << 1$

and $\frac{W_o U_o r_o}{V_o^2 r_o} = \frac{U_o}{V_o^2 r_o}\left(\frac{W_o r_o}{1}\right)$

recall $\frac{U_o}{r_o}\,\frac{Z_o}{W_o} = 1 \Rightarrow r_o W_o = U_o Z_o$

then; $\frac{U_o}{V_o^2 r_o}\left(\frac{V_o Z_o}{1}\right) = \left(\frac{U_o}{V_o}\right)^2\left(\frac{Z_o}{r_o}\right) = 0$

(0)

Now take the coefficient

$$\frac{1}{\rho}\left(\frac{P_o r_o}{r_o V_o^2}\right) = \frac{1}{\rho}\,\frac{P_o}{V_o^2} = 1 \Rightarrow P_o = \rho V_o^2$$

Now take the coefficient

$$\nu\left(\frac{U_o}{V_o^2}\right)\frac{r_o}{r_o^2} = \frac{\nu}{V_o r_o}\left(\frac{U_o}{V_o}\right)\frac{r_o}{r_o} = \frac{\nu}{V_o r_o}\left(\frac{U_o}{V_o}\right)\frac{Z_o}{Z_o}\,\frac{\nu}{r_o}\left(\frac{U_o}{V_o}\right)\frac{Z_o}{r_o} \Rightarrow 0$$

(1; 0 0)

Now the final coefficient in the radial momentum equation

$$\nu\,\frac{U_o}{Z_o^2}\,\frac{r_o}{V_o^2} = \frac{\nu}{V_o Z_o}\left(\frac{r_o}{Z_o}\right)\left(\frac{U_o}{V_o}\right) = Pv = 1$$

($>>1$; $>>1$)

Therefore the non-dimensional form of the radial momentum equation is

$$-\frac{\bar{v}^2}{\bar{r}} = -\frac{\partial \bar{P}}{\partial \bar{r}} + \frac{\partial^2 \bar{U}}{\partial \bar{Z}^2}$$

Now going to the Theta Momentum equation

$$\cancel{\frac{\alpha V}{\alpha t}} + U\frac{\alpha V}{\alpha r} + \frac{V}{r}\cancel{\frac{\alpha V}{\alpha \theta}} + W\frac{\alpha V}{\alpha Z} + \frac{VU}{r} = \frac{-1}{\rho r}\frac{\alpha \rho}{\alpha \theta} + \bar{r}_\theta$$

$$0 = \frac{\alpha}{\alpha t} \qquad \frac{\alpha}{\alpha \theta} = 0 \qquad \frac{\alpha}{\alpha \theta} = 0 \qquad \text{No body force}$$

$$+ r\left(\frac{1}{r}\frac{\alpha}{\alpha r}\left(r\frac{\alpha V}{\alpha r}\right) + \frac{1}{r^2}\cancel{\frac{\alpha^2 V}{\alpha \theta^2}} + \frac{\alpha^2 V}{\alpha Z^2} + \frac{2}{r^2}\cancel{\frac{\alpha V}{\alpha \theta}} - \frac{V_\theta}{r^2}\right)$$

$$0 = \frac{\alpha}{\alpha \theta} \qquad \frac{\alpha}{\alpha \theta} = 0$$

$$U\frac{\alpha V}{\alpha r} + W\frac{\alpha V}{\alpha Z} + \frac{VU}{r} = \nu\left(\frac{1}{r}\frac{\alpha}{\alpha r}\left(r\frac{\alpha V}{\alpha r}\right) + \frac{\alpha^2 V}{\alpha Z^2} - \frac{V}{r^2}\right)$$

Introducing non-dimensionalizing variables

$$\frac{U_o V_o}{r_o}\bar{U}\frac{\alpha \bar{V}}{\alpha \bar{r}} + \frac{W_o V_o}{Z_o}\bar{W}\frac{\alpha \bar{V}}{\alpha \bar{Z}} + \frac{V_o U_o}{r_o}\frac{\bar{V}\bar{U}}{\bar{r}} =$$

$$r\left(\frac{V_o}{r_o{}^2}\right)\frac{1}{\bar{r}}\frac{\alpha}{\alpha \bar{r}}\left(\bar{r}\frac{\alpha \bar{V}}{\alpha \bar{r}} + \frac{V_o}{Z_o{}^2}\frac{\alpha^2 \bar{V}}{\alpha \bar{Z}^2} - \frac{V_o}{r_o{}^2}\frac{\bar{V}}{\bar{r}^2}\right)$$

now divide by $\nu \frac{V_o}{Z_o{}^2}$

$$\frac{1}{\nu}\left(\frac{U_o V_o}{r_o}\frac{Z_o{}^2}{V_o}\right)\bar{U}\frac{\alpha \bar{V}}{\alpha \bar{r}} + \left(\frac{W_o V_o}{\nu Z_o}\frac{Z_o{}^2}{V_o}\right)\bar{W}\frac{\alpha \bar{V}}{\alpha \bar{Z}} + \left(\frac{V_o U_o}{\nu r_o}\frac{Z_o{}^2}{V_o}\right)\frac{\bar{V}\bar{U}}{\bar{r}} =$$

$$\left(\frac{V_o}{r_o{}^2}\frac{Z_o{}^2}{V_o}\right)\frac{1}{\bar{r}}\frac{\alpha}{\alpha \bar{V}}\left(\bar{r}\frac{\alpha \bar{V}}{\alpha \bar{r}}\right) + \frac{\alpha^2 \bar{V}}{\alpha \bar{Z}^2} - \left(\frac{V_o}{r_o{}^2}\frac{Z_o{}^2}{V_o}\right)\frac{\bar{V}}{\bar{r}^2}$$

Taking each coefficient one at a time

$$\frac{1}{r}\frac{U_o V_o}{r_o}\frac{Z_o{}^2}{V_o} = \frac{V_o Z_o}{\nu}\left(\frac{U}{V}\right)\left(\frac{Z_o}{r_o}\right) = \frac{1}{\cancel{\rho}\nu}\overset{1}{\nearrow}\left(\frac{\cancel{U_o}}{\cancel{V_o}}\right)\overset{o}{\nearrow}\left(\frac{\cancel{Z_o}}{\cancel{o}}\right)\overset{o}{\nearrow} = 0$$

Recall P_V is order 1 from radial momentum equation.

Preceeding on to the next coefficient

$$\frac{W_o V_o}{r Z_o}\left(\frac{Z_o}{V_o}\right)^2 \Rightarrow \text{recall } 1 = \frac{W_o}{Z_o} = \frac{r_o}{U_o} \Rightarrow W_o = U_o \frac{Z_o}{V_o}$$

$$\frac{W_o}{\nu}\frac{V_o}{Z_o}\left(\frac{Z_o}{V_o}\right)^2 = \frac{U_o}{r_o}\frac{V_o}{\nu}\left(\frac{Z_o}{V_o}\right)^2 = \frac{U_o}{r_o}\frac{V_o}{r}\left(\frac{Z}{V_o}\right)^2 = \frac{1}{P_V}\,\frac{U_o}{V_o}\,\frac{Z_o}{r_o}$$

($P_V \to 1$; $U_o/V_o \to 0$; $Z_o/r_o \to 0$)

$$= 0$$

Taking the next coefficient

$$\frac{V_o U_o}{\nu\, r_o}\left(\frac{Z_o}{V_o}\right)^2 = \frac{1}{P_V}\left(\frac{Z_o}{r_o}\right)\left(\frac{U_o}{V_o}\right) = 0$$

($P_V \to 1$; $Z_o/r_o \to 0$; $U_o/V_o \to 0$)

and finally the last coefficient

$$\frac{V_o}{r_o^2}\left(\frac{Z_o}{V_o}\right)^2 = \left(\frac{Z_o}{r_o}\right)^2 = 0$$

($Z_o/r_o \to 0$)

This reduces the Theta Momentum equation to $\frac{\alpha^2 \bar{V}}{\alpha Z^2} = 0$ (non-dimensional form). Finally, the axial momentum equation

$$\frac{\alpha w}{\alpha t} + \frac{U \alpha w}{\alpha r} + \frac{V}{r}\frac{\alpha w}{\alpha \theta} + w\frac{\alpha w}{\alpha Z} = -\frac{1}{\rho}\frac{\alpha P}{\alpha Z} + F_Z +$$

$\frac{\alpha w}{\alpha t} \to 0 = \frac{\alpha}{\alpha t}$; $\frac{\alpha w}{\alpha \theta} \to 0 = \frac{\alpha}{\alpha \theta}$; $F_Z \to 0 \Rightarrow$ no body forces

$$\nu\left(\frac{1}{r}\frac{\alpha}{\alpha r}\left(r\frac{\alpha w}{\alpha r}\right) + \frac{1}{r^2}\frac{\alpha^2 W}{\alpha \theta^2} + \frac{\alpha^2 W}{\alpha Z^2}\right)$$

$\frac{\alpha^2 W}{\alpha \theta^2} \to 0 = \frac{\alpha}{\alpha \theta}$

$$U\frac{\alpha W}{\alpha r} + W\frac{\alpha W}{\alpha Z} = -\frac{1}{\rho}\frac{\alpha P}{\alpha Z} + \left(\frac{1}{r_o}\ \frac{\alpha}{\alpha r}\left(r\ \frac{\alpha W}{\alpha r}\right) + \frac{^2W}{Z^2}\right)$$

Introduce non-dimensional variables

$$\frac{U_o W_o}{r_o}\left(\bar{U}\frac{\alpha \bar{W}}{\alpha \bar{r}}\right) + \frac{W_o{}^2}{Z_o}\left(\bar{W}\frac{\alpha \bar{W}}{\alpha \bar{Z}}\right) = \frac{-P_o}{\rho Z_o}\frac{\alpha \bar{P}}{\alpha \bar{Z}} +$$

$$\nu\left(\frac{W_o}{r_o{}^2}\left(\frac{1}{\bar{r}}\ \frac{\alpha}{\alpha \bar{r}}\left(\bar{r}\frac{\alpha \bar{W}}{\alpha \bar{r}}\right) + \frac{W_o}{Z_o{}^2}\ \frac{\alpha^2 \bar{W}}{\alpha \bar{Z}^2}\right)\right.$$

Now divide the above equation by $\frac{V_o{}^2}{Z_o} = \frac{P_o}{Z_o\rho}$

$$\frac{U_o W_o}{r_o}\ \frac{Z_o}{V_o{}^2}\left(\bar{U}\frac{\alpha \bar{W}}{\alpha \bar{r}}\right) + \frac{W_o{}^2}{Z_o}\ \frac{Z_o}{V_o{}^2}\left(\bar{W}\frac{\alpha \bar{W}}{\alpha \bar{Z}}\right) = -\frac{\alpha \bar{P}}{\alpha \bar{Z}}$$

$$+ \frac{W_o}{r_o{}^2}\ \frac{Z_o}{V_o{}^2}\left(\frac{1}{\bar{r}}\ \frac{\alpha}{\alpha \bar{r}}\left(\bar{r}\frac{\alpha \bar{W}}{\alpha \bar{r}}\right)\right) + \frac{\nu W_o Z_o}{Z_o{}^2 V_o{}^2}\left(\frac{\alpha^2 \bar{W}}{\alpha \bar{Z}^2}\right)$$

Now examine each coefficient separately.

$$\frac{U_o W_o}{r_o}\ \frac{Z_o}{V_o{}^2} = \left(\frac{Z_o}{V_o}\right)^2\left(\frac{U_o}{V_o}\right)^2 = 0$$

$\frac{Z_o}{V_o} \to 0$ $\quad$ $\frac{U_o}{V_o} \to 0$

next

$$\frac{W_o{}^2}{Z_o}\ \frac{Z_o}{V_o{}^2} = \left(\frac{U_o}{V_o}\right)^2\left(\frac{Z_o}{r_o}\right)^2 = 0$$

$\frac{U_o}{V_o} \to 0$

preceding on

$$\nu\ \frac{W_o}{r_o{}^2}\cdot\frac{Z_o}{V_o{}^2} = \frac{\nu(U_o\ \frac{Z_o}{r_o})\ Z_o}{r_o{}^2\ V_o{}^2} = \frac{\nu}{V_o Z_o}\left(\frac{U_o}{V_o}\right)\left(\frac{Z_o}{r_o}\right)^3 = 0$$

$\frac{U_o}{V_o} \to 0$ $\quad$ $\frac{Z_o}{r_o} \to 0$

finally

$$\frac{\nu W_o}{Z_o^2}\frac{Z_o}{V_o^2} = \frac{\nu(U_o \frac{Z_o}{r_o})Z_o}{Z_o^2 V_o^2} = \frac{\nu}{V_o Z_o}\left(\frac{U_o}{V_o}\right)\left(\frac{Z_o}{r_o}\right) = 0$$

(the $\frac{U_o}{V_o}$ factor is crossed out and annotated "o")

Therefore, the overall momentum equation is reduced to

$$0 = -\frac{\alpha P}{\alpha Z}$$

[i.e., pressure constant across the gap].

This means $\frac{\alpha \bar{P}}{\alpha \bar{r}} = \frac{d\bar{P}}{d\bar{r}}$ since

$$\frac{d\bar{P}}{\alpha\theta} = \frac{\alpha \bar{P}}{\alpha Z} = 0.$$

The set of non-dimensional governing equations to the fluid dynamics problem are:

continuity

$$\frac{1}{\bar{r}}\frac{\alpha(\bar{r}\bar{U})}{\alpha \bar{r}} + \frac{\alpha \bar{W}}{\alpha \bar{Z}} = 0$$

radial momentum

$$-\frac{V}{\bar{r}}^2 = -\frac{\alpha \bar{P}}{\alpha \bar{r}} + \frac{\alpha^2 \bar{U}}{\alpha Z}\,2$$

Theta momentum

$$0 = \frac{\alpha^2 \bar{V}}{\alpha Z^2}$$

axial momentum

$$0 = \frac{\alpha P}{\alpha Z}$$

unphysical variables

$$\frac{1}{r}\frac{\alpha(rU)}{\alpha r} + \frac{\alpha W}{dZ} = 0$$

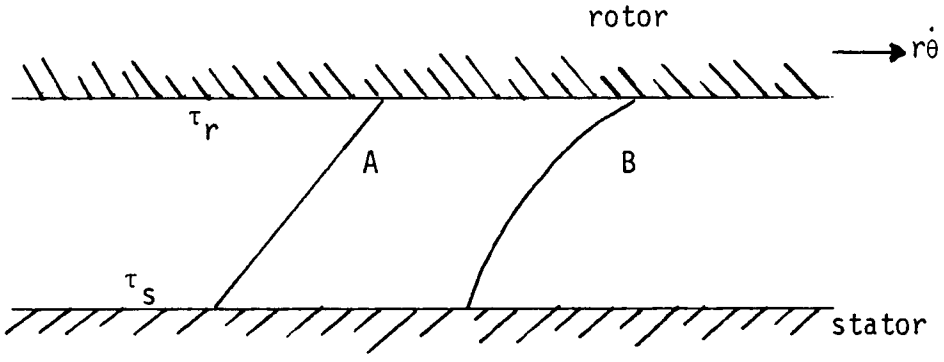
$$-\frac{V^2}{r} = -\frac{1}{\rho}\frac{dP}{dr} + r\frac{\alpha^2 U}{\alpha Z^2}$$

$$0 = \frac{\alpha^2 V}{\alpha Z^2}$$

APPENDIX B

DERIVATION OF MOMENT OF MOMENTUM EQUATION

Assuming a couette velocity profile for the tantential velocity (Curve A).



results in a zero net shear stress on the Control Volume:

$$V = \left(\frac{Z}{g}\right) r\dot{\theta} \quad => \frac{\alpha V}{\alpha Z} = \frac{r\dot{\theta}}{g}$$

$$\tau_r = \mu \frac{\alpha V}{\alpha Z}\Big|_{Z=0} = \mu \frac{r\dot{\theta}}{g}$$

$$\tau_s = -\mu \frac{\alpha V}{\alpha Z}\Big|_{Z=g} = -\mu \frac{r\dot{\theta}}{g}$$

$$\tau_r + \tau_s = \mu\left(\frac{r\dot{\theta}}{g} - \frac{r\dot{\theta}}{g}\right) = 0$$

Thus, the air has no net resisting force in the tangential direction. However, if a quadratic profile is assumed, in which the coefficients are functions of r (figure, : Curve B), the magnitudes of the shear stresses on the rotor and stator may be different as shown below:

$$V = bZ + c\,Z^2 => \frac{\alpha V}{\alpha Z} = b + 2\,C\,Z$$

$$\tau_s = \mu \frac{\alpha V}{\alpha Z}\Big|_{Z=0} = \mu b$$

$$\tau_r = -\mu \frac{\alpha V}{\alpha Z}\Big|_{Z=s} = -(b + 2cg)\mu$$

$$\tau_r + \tau_s = -2cg$$

Thus, the net shear stress on the Control Volume is not zero for the quadratic profile.

Now by application of the Moment of Momentum equation

$$\Gamma = \dot{m}\,(V_{out}\, r_{out} - V_{in}\, r_{in})$$

APPENDIX C

FLOW REGIME

Calibration of the surface probe was based on the assumption of fully-developed flow. Therefore, knowing where the radial flow could be assumed fully developed was imperative. The hydrodynamic entry length was obtained by the following equation: (reference 11 and 12)

$$\frac{Re_Q}{20} = \frac{X}{D}$$

where Re_Q is based on volumeteric flow and r_il D is equal to the gap width (D=g) and X is the hydrodynamic entry length measured in a radial direction beginning from the inner radius (r_i) of the test section.

$$Re_Q = \frac{U_r\, g}{\nu}$$

where

$$U_r = \frac{Q}{2\pi r_1 g}$$

therefore

$$Re_Q = \frac{Q}{2\pi r_1 \nu}$$

substituting

$$\frac{Q}{2\pi r_1 \nu}\left(\frac{1}{20}\right) = \frac{X}{g}$$

$$\frac{Qg}{40\pi r_1 \nu} = X$$

combining

$$\frac{Qg}{37.6} = X$$

Calibration of the surface probe took place in gaps ranging from 0.010 - 0.020 inches and air volumeteric flow rates up to 400 SCFH. Therefore, the longest hydroynamic entry length corresponded to a flow

rate of 400 SCFH and a gap of 0.020 inches. Thus X equals 0.0177 of an inch. This clearly places the positions of all the hot film surface probe mounts in the full-developed flow regime.

APPENDIX D

DATA UNCERTAINTY ANALYSIS

In any study where data is recorded an estimate of the uncertainty of each measurement and how that measurement will effect the final result is import. This experiment assumed the following list of inherent errors in the text rig or in data acquistion:

Measurement	Uncertainty
Air Flow Rate	± 5 SCFH
Gap Setting	± 0.001 inches
Radial Distance	± 0.0005 inches
Hot Film Surface	
Probe Voltage	± 0.005 volts

The uncertainty in the reading the hot film surface probe voltage results in the following uncertainty in obtaining the local shear stress from the hot film surface probe's calibration curve:

Voltage Range	Uncertainty
13.1 - 13.2	0.5×10^{-3} (lb/ft^2)
13.2 - 13.3	2.5×10^{-3} (lb/ft^2)
13.3 - 13.4	4.0×10^{-3} (lb/ft^2)

Since the quadratic assumption made only second order corrections to the couette approximation and since the equation developed in this investigation required numerical techniques to solve for the pressure, the equation developed by Pelech and Sharpio will be used to estimate the uncertainty of the pressure data. The equation they developed is given by:

$$P = \left(\frac{3}{20}\right) \rho \dot{\theta}^2 r^2 - \frac{6\mu Q}{\pi g^2} \ln r$$

To obtain this estimate of the uncertainty, the method developed by Kline and McClintock[13] will be followed. This method essentially consists of summing the squares of the uncertainties of each primary measurement, then taking the square root of this sum. The influence of each measurement upon the uncertainty of the final result is obtained by taking the partial derivative of the final result with respect to each measurement and then multiplying that derivative times the possible error in that measurement. (This is the item that is squared.) These quantities were obtained for six different variables in the equation given above. The partial derivatives are listed below:

$$\frac{dP}{dr} = \left(\frac{3}{20}\right) \rho \dot{\theta}^2 r - \frac{6Q\mu}{\pi r g^3}$$

$$\frac{dP}{dQ} = - \frac{6\mu}{\pi g^3} \ln r$$

$$\frac{dP}{d\mu} = - \frac{6Q}{\pi g^3} \ln r$$

$$\frac{dP}{d\dot{\theta}} = \left(\frac{3}{10}\right) \rho \dot{\theta} r^2$$

$$\frac{dP}{dg} = - \frac{18\mu Q}{\pi s^4} \ln r$$

$$\frac{dP}{dP} = \frac{3}{20} \dot{\theta}^2 r^2$$

In the above mentioned equation the value used for ρ was 0.0763 lb_m/ft^3 and the value used for μ was 0.0453 $lb_m/(ft\text{-}sec)$. In the uncertainty

analysis these values were assumed to be known within 10 per cent. The partial derivatives also gives an indication of how the dependent final result is on the measurement. The numerical values of the partial derivatives are listed below for 50 SCFH, gap width = 0.010 inches and a rotor's speed of 500 RPM.

$$\frac{dP}{dr} = -\ 27\ \frac{lb}{f+3}$$

$$\frac{dP}{dQ} = 606\ \frac{lb\ -\ sec}{f+5}$$

$$\frac{dP}{d\theta} = 0.0145\ \frac{lb\ -\ sec}{f+2\ -\ rad}$$

$$\frac{dP}{dg} = 30.308(10)^{3}\ \frac{lb}{f+3}$$

$$\frac{dP}{dP} = 160\ \frac{f+^{2}}{sec^{2}}$$

$$\frac{\alpha P}{\alpha \mu} = -21(10)^{6}\ \frac{1}{sec}$$

The dependence on the gap width was not surprising, since the data showed the same trend. Table 1 lists the uncertainty of the pressure measurements (in inches of water).

TABLE 1

PRESSURE UNCERTAINTY
(IN INCHES OF WATER) vs.
FLOW LOCATION

Q SCFH	500 RPM	1000 RPM	1500 RPM	2000 RPM	2500 RPM	3000 RPM
			Gap Width = 0.010 inches			
50	0.33	0.34	0.34	0.35	0.38	0.43
200	1.18	1.18	1.18	1.18	1.19	1.21
300	1.76	1.76	1.76	1.76	1.77	1.78
			Gap Width = 0.014 inches			
50	0.10	0.11	0.12	0.16	0.21	0.28
200	0.35	0.35	0.36	0.37	0.40	0.44
300	0.52	0.52	0.53	0.54	0.55	0.58
			Gap Width = 0.020 inches			
50	0.03	0.04	0.07	0.12	0.18	0.26
200	0.10	0.11	0.12	0.16	0.21	0.28
300	0.15	0.16	0.17	0.19	0.24	0.30

APPENDIX E

COMPUTER PROGRAM

```
UNIVERSITY OF PITTSBURGH, DECSYSTEM-10

CSMP -- CONTINUOUS SYSTEM MODELING PROGRAM

VERSION 1.3 (17-MAR-78)



INITIAL
*
*       CHANGING INDEPENT VARIABLE
*
RENAME  TIME=AS
*
*       SETTING PARAMETERS AND CONSTANTS
*
CONSTANT OR=7.5   , IR=5.85,   PI=3.14159
CONSTANT G=0.016  , D=300.
*       MU UNITS ARE FT*FT/HR   MU UNITS ARE LB/FT*HR
CONSTANT NU=0.61943   , MU=0.0453
CONSTANT RPM=3000.
*
*       SETTING NON-DIMENSIONAL GROUPS
*
*       GAP RATIO
TH=G/OR
*       RE = REYNOLDS NUMBER = D*RO/2*PI*G*PI*MU
RE=3.9699*(D/G)
*       RR = RADIUS RATIO = RI/RO
RR=IR/OR
*       PV=MU/AMEGA*RO*G
PV=3.3030E-3*(1./(G*AMEGA))
K=128./(RE*TH*TH*RR)
*       SETTING DIMENSIONAL GROUPS
AMEGA=RPM*PI/30.
CO=90.*AMEGA/G
*       TORQUE IS IN PSF
TO=8.0606391E-6*MU*AMEGA/TH
*       PRESSURE IS IN INCHES OF WATER
*       PO= ( DENSITY ) * VO *VO
PO=RPM*RPM/524869.32
*
DYNAMIC
*
R=AS+RR
CB=3.*(1.-EXP((K/2.)*(RR*RR-R*R)))/(K*R)
C=CO*CB
*       QUADRATIC  NON-DIMENSIONAL TORQUE
TD=R-CB
*       PELECH & SHAPIRO'S NON-DIMENSIONAL TORQUE
TOP = R
T1=TD*TO
T2=TOP*TO
DPB1=(0.3*R-CB/(5.)+3.*CB*CB/(70.*R)-12.*RE*RR*PV*PV/R)
PB1=INTGRL(0.0,DPB1)
*       PELECH & SHAPIRO'S NON-DIMENSIONAL PRESSURE
DPB2 = (0.3*R)-12.*RE*RR*PV*PV/R
PB2 = INTGRL (0.0, DPB2)
```

```
B2 = P02*P0
*       ERRORES BETWEEN P&S'S PRESSURE & PRESSURES & TORUES
*                          AND THE QUADRATIC'S
ERROR = (1. - (PB/B2))*100.
RROR = (1. - (TD/TOP))*100.
PB=P0*PB1
TIMER FINTIM=0.22  ,PRDEL=0.01
*
TERMINAL
*
PRINT R, TD,TOP,T1,PB,B2,ERROR,RROR,C
END
STOP
```

```
OUTPUT VARIABLE SEQUENCE
AMEGA   PV      PR      TM      RE      X       CO      TO      P0      R
C3      DPB1    P01     DPB2    PB2     C       TD      T1      TOP     T2
B2      PB      ERROR   RROR
```

```
 OUTPUTS     INPUTS    PARAMS  INTEGS + MEM BLKS  FORTRAN  DATA CDS
 28(500)   74(1400)   10(400)   2+  0=  2(300)    25(600)       7
```

```
ENDJOB
```

APPENDIX F

DATA

TABLE 2

AVERAGE PRESSURE DATA IN INCHES IN WATER

Pressure Taps	500 RPM	1000 RPM	1500 RPM	2000 RPM	2500 RPM	2500 RPM
Flow Rate = 50 SCFH					Gap = 0.010 inches	
1	0.75	0.61	0.37	0.04	-0.37	-0.91
2	0.73	0.64	0.49	0.29	0.06	-0.21
3	0.52	0.45	0.33	0.19	0.01	-0.21
4	0.32	0.26	0.19	0.10	-0.02	-0.17
5	0.15	0.125	0.09	0.04	-0.03	-0.10
6	0.08	0.067	0.04	-0.02	-0.04	-0.09
7	0.05	0.04	0.02	-0.02	-0.05	-0.08
8	0.04	0.03	0.02	-0.005	-0.01	-0.02
9	0.03	0.02	0.01	0	-0.2	-0.03
Flow Rate = 200 SCFH					Gap = 0.010 inches	
1	--	2.81	2.50	2.17	1.76	1.33
2	2.68	2.59	2.35	2.12	1.87	1.57
3	1.96	1.82	1.64	1.48	1.26	1.04
4	1.18	1.13	1.00	0.89	0.75	0.60
5	0.54	0.51	0.44	0.38	0.31	0.24
6	0.28	0.25	0.22	0.17	0.13	0.07
7	0.18	0.17	0.13	0.09	0.07	0.03
8	0.12	0.11	0.09	0.07	0.06	0.04
9	0.09	0.08	0.05	0.05	0.03	0.02
Flow Rate = 300 SCFH					Gap = 0.010 inches	
1	+3	+3	+3	+3	+3	2.72
2	+3	+3	+3	+3	2.96	2.63
3	2.71	2.69	2.44	2.24	2.07	1.76
4	1.70	1.66	1.51	1.37	1.25	1.04
5	0.77	0.74	0.65	0.58	-.52	0.42
6	0.40	0.37	0.30	0.25	0.21	0.16
7	0.26	0.24	0.18	0.14	0.12	0.08
8	0.16	0.14	0.11	0.08	0.07	0.05
9	0.11	0.10	0.06	0.04	0.03	0.02

TABLE 2 (Continued)

Pressure Taps	500 RPM	1000 RPM	1500 RPM	2000 RPM	2500 RPM	2500 RPM
Flow Rate = 50 SCFH					Gap = 0.014 inches	
1	0.27	0.15	-0.07	-0.41	-0.83	-1.35
2	0.28	0.19	0.06	-0.12	-0.35	-0.61
3	0.20	0.13	0.03	-0.10	-0.29	-0.49
4	0.13	0.08	0.02	-0.08	-0.21	-0.34
5	0.07	0.04	0.01	-0.04	-0.11	-0.17
6	0.04	0.02	0.	-0.03	-0.08	-0.11
7	0.03	0.015	0.	-0.02	-0.06	-0.08
8	0.02	0.01	0.	-0.01	-0.03	-0.03
9	0.02	0.01	0.	-0.01	-0.02	-0.04
Flow Rate = 200 SCFH					Gap = 0.014 inches	
1	1.23	1.12	0.89	0.62	0.23	-0.29
2	1.11	1.01	0.88	0.68	0.43	0.09
3	0.81	0.73	0.62	0.48	0.28	0.04
4	0.51	0.46	0.38	0.28	0.16	0.01
5	0.23	0.21	0.17	0.12	0.06	-0.02
6	0.13	0.11	0.08	0.05	0.01	-0.02
7	0.09	0.07	0.05	0.03	0.01	-0.03
8	0.06	0.05	0.03	0.02	0.01	-0.01
9	0.05	0.04	0.02	0.01	0.005	-0.01
Flow Rate = 300 SCFH					Gap = 0.014 inches	
1	2.05	1.92	1.70	1.37	1.04	0.55
2	1.77	1.65	1.49	1.28	1.00	0.68
3	1.27	1.18	1.04	0.88	0.68	0.44
4	0.81	0.76	0.65	0.53	0.40	0.25
5	0.38	0.33	0.28	0.22	0.16	0.08
6	0.20	0.17	0.13	0.09	0.07	0.015
7	0.13	0.10	0.08	0.05	0.03	0.005
8	0.09	0.07	0.05	0.03	0.02	0
9	0.07	0.04	0.03	0.02	0.005	-0.01

TABLE 2 (Continued)

Pressure Taps	500 RPM	1000 RPM	1500 RPM	2000 RPM	2500 RPM	2500 RPM
Flow Rate = 50 SCFH					Gap = 0.016 inches	
1	0.18	0.05	-0.17	-0.49	-0.90	-1.40
2	0.18	0.10	-0.03	-0.20	-0.43	-0.69
3	0.13	0.07	-0.03	-0.16	-0.34	-0.53
4	0.08	0.04	-0.03	-0.11	-0.23	-0.36
5	0.04	0.02	-0.02	-0.06	-0.12	-0.18
6	0.02	0.02	-0.02	-0.04	-0.08	-0.13
7	0.015	0.01	-0.01	-0.03	-0.06	-0.10
8	0.01	0.01	0	-0.015	-0.03	-0.04
9	0.01	0.005	-0.005	-0.01	-0.03	-0.05
Flow Rate = 200 SCFH					Gap = 0.016 inches	
1	0.83	0.69	0.52	0.24	-0.15	-0.60
2	0.73	0.65	0.51	0.33	0.08	-0.17
3	0.54	0.47	0.37	0.22	0.04	-0.15
4	0.34	0.29	0.23	0.05	0	-0.12
5	0.16	0.13	0.10	0.05	-0.005	-0.07
6	0.09	0.07	0.50	0.002	-0.02	-0.06
7	0.05	0.05	0.03	0.01	-0.02	-0.04
8	0.04	0.03	0.02	0.01	-0.01	-0.02
9	0.03	0.02	0.01	0	-0.01	-0.02
Flow Rate = 300 SCFH					Gap = 0.016 inches	
1	1.38	1.26	1.07	0.81	0.46	0.05
2	1.16	1.07	0.92	0.73	0.49	0.23
3	0.85	0.76	0.65	0.50	0.32	0.13
4	0.54	0.48	0.38	0.30	0.18	0.06
5	0.25	0.22	0.17	0.12	0.07	0.005
6	0.14	0.11	0.08	0.05	0.02	-0.02
7	0.09	0.06	0.04	0.02	0.01	-0.02
8	0.06	0.04	0.02	0.02	-0.005	-0.01
9	0.04	0.03	0.01	0	0.005	-0.01

TABLE 2 (Continued)

Pressure Taps	500 RPM	1000 RPM	1500 RPM	2000 RPM	2500 RPM	2500 RPM
Flow Rate = 50 SCFH					Gap = 0.20 inches	
1	0.07	-0.05	-0.27	-0.58	-0.97	-1.45
2	0.07	-0.01	-0.13	-0.29	-0.51	-0.76
3	0.05	-0.005	-0.10	-0.23	-0.40	-0.58
4	0.03	-0.005	-0.10	-0.23	-0.40	-0.58
5	0.02	-0.005	-0.04	-0.09	-0.14	-0.20
6	0.01	-0.005	-0.03	-0.05	-0.10	-0.12
7	0	-0.05	-0.02	-0.04	-0.09	-0.10
8	0.005	-0.005	-0.015	-0.03	-0.03	-0.04
9	0.005	0	-0.01	-0.02	-0.04	-0.05
Flow Rate = 200 SCFH					Gap = 0.020 inches	
1	0.41	0.31	0.14	-0.12	-0.46	-0.84
2	0.36	0.30	0.16	-0.02	-0.19	-0.39
3	0.25	0.20	0.11	-0.02	-0.16	-0.31
4	0.16	0.12	0.06	-0.03	-0.12	-0.21
5	0.07	0.06	0.03	-0.02	-0.07	-0.11
6	0.04	0.03	0.01	-0.02	-0.05	-0.08
7	0.03	0.02	0	-0.02	-0.04	-0.07
8	0.02	0.01	0	-0.01	-0.02	-0.02
9	0.01	0.01	0	-0.01	-0.02	-0.03
Flow Rate = 300 SCFH					Gap = 0.020 inches	
1	0.71	0.64	0.45	0.21	-0.08	-0.39
2	0.58	0.52	0.38	0.21	-0.03	-0.13
3	0.41	0.36	0.25	0.13	-0.02	-0.10
4	0.26	0.21	0.15	0.06	-0.02	-0.08
5	0.12	0.10	0.06	0.02	-0.02	-0.05
6	0.07	0.04	0.03	0	-0.02	-0.03
7	0.04	0.02	0.02	0	-0.02	-0.03
8	0.03	0.01	0.01	0	-0.01	-0.01
9	0.02	0.01	0.005	-0.005	-0.01	-0.01

TABLE 3

AVERAGED TANGENTIAL SHEAR STRESS DATA
IN VOLTS

Position	500 RPM	1000 RPM	1500 RPM	2000 RPM	2500 RPM	2500 RPM
Flow Rate = 50 SCFH					Gap = 0.010 inches	
Inner	13.257	13.342	13.404	13.453	13.494	13.528
Middle	13.309	12.392	13.453	13.499	13.537	13.571
Outer	13.221	13.294	13.344	13.382	13.411	13.435
Flow Rate = 200 SCFH					Gap = 0.010 inches	
Inner	13.349	13.388	13.430	13.468	13.502	13.532
Middle	13.397	13.438	13.478	13.514	13.546	13.571
Outer	13.290	13.326	13.358	13.367	13.411	13.431
Flow Rate - 300 SCFH					Gap = 0.010 inches	
Inner	13.411	13.479	13.459	13.487	13.515	13.540
Middle	13.457	13.479	13.507	13.533	13.559	13.584
Outer	13.340	13.359	13.380	13.399	13.417	13.431
Zero Pressure Difference					Gap = 0.010 inches	
Inner	13.242	13.338	13.402	13.451	13.477	13.524
Middle	13.296	13.385	13.447	13.495	13.534	13.564
Outer	13.256	13.334	13.388	13.425	13.454	13.477
Flow Rate = 50 SCFH					Gap = 0.014 inches	
Inner	13.214	13.291	13.348	13.393	13.430	13.462
Middle	13.256	12.333	13.387	13.430	13.466	13.495
Outer	13.180	13.248	13.297	13.355	13.362	13.386
Flow Rate = 200 SCFH					Gap = 0.014 inches	
Inner	13.280	13.323	13.364	13.400	13.435	13.464
Middle	13.319	13.363	13.403	13.439	13.470	13.495
Outer	13.232	13.268	13.302	13.337	13.355	13.424

TABLE 3 (CONTINUED)

Position	500 RPM	1000 RPM	1500 RPM	2000 RPM	2500 RPM	2500 RPM
Flow Rate - 300 SCFH					Gap = 0.014 inches	
Inner	13.320	13.354	13.382	13.413	13.422	13.467
Middle	13.365	13.390	13.420	13.451	13.477	13.383
Outer	13.273	13.294	13.317	13.339	13.358	13.374
Zero Pressure Difference					Gap = 0.014 inches	
Inner	13.198	13.283	13.340	13.376	13.412	13.442
Middle	13.248	13.330	13.386	13.428	13.462	13.492
Outer	13.178	13.253	13.301	13.381	13.397	13.417
Flow Rate = 50 SCFH					Gap = 0.016 inches	
Inner	13.20	13.277	13.332	13.377	13.413	13.446
Middle	13.207	12.280	13.332	13.372	13.407	13.435
Outer	13.232	13.299	13.345	13.381	13.409	13.579
Flow Rate = 200 SCFH					Gap = 0.016 inches	
Inner	13.258	13.303	13.346	13.383	13.415	13.442
Middle	13.258	13.301	13.351	13.377	13.408	13.433
Outer	13.325	13.309	13.345	13.375	13.399	13.423
Flow Rate - 300 SCFH					Gap = 0.016 inches	
Inner	13.304	13.330	13.360	13.393	13.420	13.445
Middle	13.297	13.323	13.362	13.384	13.414	13.350
Outer	13.305	13.329	13.354	13.378	13.398	13.417
Zero Pressure Difference					Gap = 0.016 inches	
Inner	13.196	13.278	13.332	13.385	13.423	13.455
Middle	13.192	13.270	13.323	13.363	13.399	13.429
Outer	13.227	13.298	13.343	13.330	13.361	13.375

TABLE 3 (Continued)

Position	500 RPM	1000 RPM	1500 RPM	2000 RPM	2500 RPM	2500 RPM
Flow Rate = 50 SCFH					Gap = 0.020 inches	
Inner	13.212	13.215	13.341	13.377	13.424	13.539
Middle	13.108	12.239	-	-	-	-
Outer	13.177	13.235	13.274	13.305	13.491	13.574
Flow Rate = 200 SCFH					Gap = 0.020 inches	
Inner	13.248	13.297	13.341	13.347	13.411	13.514
Middle	13.239	13.244	-	-	-	-
Outer	13.203	13.239	13.269	13.294	13.367	13.563
Flow Rate - 300 SCFH					Gap = 0.020 inches	
Inner	13.282	13.311	13.347	13.351	13.411	13.485
Middle	13.268	-	-	-	-	-
Outer	13.229	13.264	13.269	13.287	13.341	13.551
Zero Pressure Difference					Gap = 0.020 inches	
Inner	13.184	13.289	13.339	13.378	13.385	13.465
Middle	13.170	13.240	13.288	13.326	13.353	13.419
Outer	13.175	13.233	13.266	13.293	13.337	13.534

TABLE 4

AVERAGED RADIAL SHEAR STRESS DATA
IN VOLTS

Position	500 RPM	1000 RPM	1500 RPM	2000 RPM	2500 RPM	2500 RPM
Flow Rate = 50 SCFH					Gap = 0.010 inches	
Inner	13.221	13.276	13.318	13.351	13.376	13.397
Middle	13.301	12.361	13.408	13.447	13.479	13.506
Outer	13.215	13.262	13.296	13.324	13.346	13.364
Flow Rate = 200 SCFH					Gap = 0.010 inches	
Inner	13.344	13.358	13.375	13.390	13.404	13.416
Middle	13.453	13.468	13.487	13.507	13.526	13.543
Outer	13.329	13.337	13.347	13.357	13.366	13.372
Flow Rate - 300 SCFH					Gap = 0.010 inches	
Inner	13.420	13.460	13.429	13.437	13.441	13.446
Middle	13.540	13.546	13.555	13.565	13.574	13.584
Outer	13.398	13.396	13.397	13.397	13.398	13.398
Zero Pressure Difference					Gap = 0.010 inches	
Inner	13.198	13.264	13.311	13.343	13.372	13.397
Middle	13.245	13.339	13.395	13.438	13.473	13.504
Outer	13.189	13.250	13.292	13.322	13.344	13.362
Flow Rate = 50 SCFH					Gap = 0.014 inches	
Inner	13.191	13.291	13.348	13.393	13.430	13.462
Middle	13.252	12.311	13.356	13.392	13.422	13.447
Outer	13.194	13.242	13.278	13.305	13.327	13.351
Flow Rate = 200 SCFH					Gap = 0.014 inches	
Inner	13.284	13.302	13.320	13.337	13.351	13.365
Middle	13.363	13.381	13.404	13.426	13.446	13.453
Outer	13.278	13.289	13.304	13.317	13.329	13.337

TABLE 4 (CONTINUED)

Position	500 RPM	1000 RPM	1500 RPM	2000 RPM	2500 RPM	2500 RPM
Flow Rate - 300 SCFH					Gap = 0.014 inches	
Inner	13.350	13.355	13.363	13.376	13.377	13.383
Middle	13.435	13.443	13.453	13.466	13.477	13.488
Outer	13.353	13.337	13.346	13.344	13.348	13.352
Zero Pressure Difference					Gap = 0.014 inches	
Inner	13.177	13.240	13.283	13.315	13.342	13.364
Middle	13.222	13.295	13.376	13.385	13.421	13.456
Outer	13.178	13.235	13.274	13.301	13.321	13.335
Flow Rate = 50 SCFH					Gap = 0.016 inches	
Inner	13.176	13.226	13.265	13.296	13.288	13.375
Middle	13.228	12.286	13.328	13.366	13.395	13.434
Outer	13.163	13.211	13.246	13.274	13.296	13.476
Flow Rate = 200 SCFH					Gap = 0.016 inches	
Inner	13.254	13.273	13.291	13.368	13.324	13.338
Middle	13.325	13.345	13.368	13.371	13.410	13.476
Outer	13.235	13.248	13.268	13.277	13.292	13.365
Flow Rate - 300 SCFH					Gap = 0.016 inches	
Inner	13.314	13.319	13.328	13.335	13.342	13.350
Middle	13.391	13.399	13.410	13.422	13.435	13.447
Outer	13.287	13.288	13.293	13.294	13.303	13.337
Zero Pressure Difference					Gap = 0.016 inches	
Inner	13.159	13.220	13.261	13.293	13.318	13.341
Middle	13.213	13.280	13.328	13.368	13.405	13.437
Outer	13.153	13.208	13.245	13.270	13.288	13.337

TABLE 4 (Continued)

Position	500 RPM	1000 RPM	1500 RPM	2000 RPM	2500 RPM	2500 RPM
Flow Rate = 50 SCFH					Gap = 0.020 inches	
Inner	13.157	13.208	13.245	13.275	13.366	13.466
Middle	13.187	12.243	13.283	13.316	13.381	13.476
Outer	13.165	13.211	13.271	13.299	13.429	13.490
Flow Rate = 200 SCFH					Gap = 0.020 inches	
Inner	13.216	13.237	13.255	13.272	13.293	13.440
Middle	13.260	13.282	13.304	13.326	13.344	13.447
Outer	13.218	13.243	13.254	13.267	13.317	13.493
Flow Rate - 300 SCFH					Gap = 0.020 inches	
Inner	13.266	13.272	13.281	13.381	13.303	13.409
Middle	13.312	13.322	13.333	13.346	13.361	13.438
Outer	13.268	13.266	13.272	13.279	13.300	13.482
Zero Pressure Difference					Gap = 0.020 inches	
Inner	13.156	13.206	13.243	13.273	13.302	13.430
Middle	13.176	13.239	13.286	13.326	13.363	13.419
Outer	13.157	13.208	13.244	13.265	13.294	13.475

TABLE 5

AVERAGED ZERO PRESSURE DIFFERENCE DATA
PRESSURES IN INCHES OF WATER
FLOW RATES IN SCFH
(Q)

Pressure Taps	500 RPM	1000 RPM	1500 RPM	2000 RPM	2500 RPM	2500 RPM
			Gap = 0.010 inches			
1	--	--	--	--	--	--
2	0	0	0	0	0	0
3	0	0	-0.05	-0.015	-0.04	-0.04
4	0.01	0	-0.015	-0.04	-0.04	-0.05
5	0	0	-0.01	-0.02	-0.03	-0.03
6	0.005	0	-0.01	-0.02	-0.04	-0.04
7	0	0	-0.01	-0.03	-0.05	-0.05
8	0	0	0	-0.01	-0.02	-0.02
9	0	0	-0.005	-0.01	-0.01	0.01
Q	0 - 3	6.8	17	30	44	75
			Gap = 0.20 inches			
1	-	-	-	-	-	-
2	0	0	0	0	0	0
3	0	0	-0.01	-0.01	-0.02	-0.03
4	0	0	-0.01	-0.02	-0.03	-0.04
5	0	0	-0.005	-0.01	-0.02	-0.04
6	0	0	-0.005	-0.01	-0.03	-0.04
7	0	0	-0.005	-0.01	-0.02	-0.04
8	0	0	0	0	-0.01	-0.02
9	0	0	0	0	-0.01	-0.02
G	4.0	18	42	75	125	190

TABLE 6

AVERAGED ZERO PRESSURE DIFFERENCE DATA
PRESSURES IN INCHES OF WATER
FLOW RATES IN SCFH
(Q)

Pressure Taps	500 RPM	1000 RPM	1500 RPM	2000 RPM	2500 RPM	2500 RPM
			Gap = 0.016 inches			
1	--	--	--	--	--	--
2	0	0	0	0	0	0
3	0	0	0	-0.01	-0.02	-0.02
4	0	0	-0.01	-0.01	-0.03	-0.03
5	0	0	-0.01	-0.01	-0.01	-0.04
6	0	0	-0.01	-0.01	-0.02	-0.03
7	0	0	-0.01	0	0.02	-0.03
8	0	0	0	0	-0.01	-0.01
9	0	0	0	0	-0.01	0.02
0	7	27.5	60	115	180	260
			Gap = 0.20 inches			
1	-	-	-	-	-	-
2	0	0	0	0	0	0
3	0	0	0	-0.01	-0.02	-0.01
4	0	0	-0.005	-0.02	-0.03	-0.01
5	0	0	-0.005	-0.01	-0.03	-0.01
6	0	0	-0.005	-0.01	-0.02	-0.02
7	0	0	-0.005	-0.01	-0.02	-0.02
8	0	0	0	-0.005	-0.01	0
9	0	0	0	0	-0.01	-0.01
G	12	52	125	212	302	350

TABLE 7

DIRECTIONAL DATA FROM FLUSH SURFACE PROBE
IN VOLTS

Degrees	50 SCFH	100 SCFH	150 SCFH	200 SCFH	250 SCFH	300 SCFH
			Gap Width = 0.010 inches			
0	13.172	13.231	13.274	13.310	13.343	13.369
45	13.193	12.255	13.279	13.345	13.379	13.407
90	13.209	13.275	13.300	13.368	13.404	13.434
			Gap Width = 0.014 inches			
0	13.131	13.171	13.203	13.229	13.250	13.264
45	13.149	13.196	13.234	13.266	13.298	13.316
90	13.163	13.215	13.254	13.288	13.316	13.340
			Gap Width = 0.016 inches			
0	13.114	13.153	13.182	13.206	13.223	13.237
45	13.128	13.170	13.200	13.227	13.248	13.262
90	13.141	13.188	13.221	13.249	13.272	13.288
			Gap Width = 0.020 inches			
0	13.096	13.129	13.155	13.176	13.192	13.204
45	13.113	13.148	13.174	13.197	13.214	13.228
90	13.125	13.161	13.190	13.213	13.230	13.241

APPENDIX G

CALIBRATION PROCEDURE FOR SURFACE PROBE

The manometers used for pressure readings were checked before each series of tests to ensure they were level and the scale was zeroed.

The calibration procedure for the hot film surface probe consisted of the following steps:

1) Set the thermo system power supply on standby.
2) Adjust the power supply reference set until the meter indicates 2 volts.
3) Adjust the probe resistance until pushing the temperature resistance measurement toggle switch makes no resulting deflection in the voltage meter.
4) The probe resistance to be set in for operation is then given by the probe resistance set in step (3), divided by the ice point resistance of the probe and then multiplied by the operating resistance of the probe. The last two resistances are specified by the manufacturer for the specific probe in use.
5) Set in the final probe resistance found in step (5).
6) Readjust the reference set on the power supply until the voltage on the meter indicates 2 volts.
7) Set power supply to run.
8) Adjust signal conditioner suppression as desired.

The probe is ready to take data at this point.

APPENDIX H

DERIVED EXPRESSIONS

Taking the assumed tangential velocity distribution $V = bZ + cZ^2$.

Relating b + c by the following boundary condition $v = r\theta$ at $Z = g$.

$$\frac{\dot{r\theta}}{g} = b + cg$$

From the radial momentum equation and substituting in the velocity profile

$$\frac{-V^2}{r} = \frac{-1}{\rho}\frac{dP}{dr} + \frac{\nu\alpha^2 U}{\alpha Z^2}$$

$$\frac{\alpha^2 U}{\alpha Z^2} = \frac{1}{\mu}\frac{dP}{dr} - \frac{1}{\nu r}(b^2y^2 + 2bcy^3 + c^2y^4)$$

Integrating with respect to Z (axial coordinate) twice

$$U = \frac{Z^2}{2\mu}\frac{dP}{dr} - \frac{1}{\nu r}\left(\frac{b^2Z^4}{12} + \frac{2bcZ^5}{20} + \frac{C^2Z^6}{30}\right) + dZ + e$$

Solving for the constants d and e from boundary condition

$$\text{at } y = 0 \quad U = 0 \Rightarrow \quad e = 0$$

$$\text{at } y = 0 \quad U = 0 \Rightarrow \quad d =$$

$$d = \frac{1}{\nu r}\left(\frac{b^2g^3}{1\alpha} + \frac{2bcg^4}{20} + \frac{C^2g^5}{30}\right) - \frac{g}{2\mu}\frac{dP}{dr}$$

Therefore, U is given by

$$U = \frac{dP}{dr}\left(\frac{Z - g}{2\mu}\right)Z - \frac{1}{\nu}\left(b^{2(g^3 - Z^3)} + \frac{2bc(g^4 - Z^4)}{20}\right.$$

$$\left. + \frac{C^2(g^5 - Z^5)}{3C}\right)\frac{Z}{r}$$

The average U is given by

$$dA = 2\pi r dZ$$

$$A = 2\pi rg$$

$$U_{ar} = \frac{1}{A}\int UdA$$

or

$$U_{AV} = \frac{Q}{2\pi rg} \text{ (from conservation of mass)}$$

$$U_{AV} = \frac{1}{\alpha\pi rg} \quad 2\pi r \left(\frac{dP}{dr}\left(\frac{y^2 - gZ}{2\ \mu}\right)\right.$$

$$+ \frac{1}{\nu}\left(\frac{b^2(g^3Z - Z^4)}{12} + \frac{2bc\ (g^4Z - Z^5)}{20}\right.$$

$$+ \frac{C^2(g^5\ Z - Z^6)}{30}\ \frac{1}{r}\ dZ$$

$$U = \frac{dP}{dr}\left(-\frac{1}{12\mu}\right) g^2 + \frac{1}{\nu}\left(\frac{3b^2g^4}{120} - \frac{4bcg^5}{120} + \frac{C^2g^6}{84}\right)\frac{1}{r}$$

$$= Q/(2\pi rg)$$

Setting the two equations for U_{AV} equal

$$\frac{Q}{2\pi rg} = \frac{dP}{dr}\left(\frac{-g^2}{12\mu}\right) + \frac{1}{\nu r}\left(\frac{3b^2g^4}{120} + \frac{4bcg^5}{120} - \frac{C^2g^6}{84}\right)$$

Solving for $\frac{dP}{dr}$

$$\frac{dP}{dr} = \rho\ \left[\frac{3r\theta^2}{10} - \frac{\theta g^2 C}{5} + \frac{3C^2g^4}{7Ur}\right) - \frac{6Qr}{\pi Vg^3}]$$

Solving for C form Moment of Momentum shear stress $\rightarrow \tau = \mu \frac{dU}{dZ}$

The net tangential shear stress applied to control volume

$$\tau_{net} = (\tau_r - \tau_s) = \mu(b + 2\ cg - b) = \mu 2cg$$

$$\int_{r_1}^{r_o} \tau_{net}\ (2\pi rr)dr = \rho\dot{m}(V_{\theta_{out}}V_{out} - \cancel{V_{\theta_{in}}\ r_{\theta_{in}}})$$

Substituting into Moment of Momentum Equation

$$= \nu_o\ \dot{m}\ V_o$$

$$2Cg\mu 2\pi r^2 dr = \frac{\rho Q}{g} r \int_0^g (by + cy^2)dy$$

$$4g\pi\mu \int Cr^2 dr = \rho Qr \left(\frac{r\dot{\theta}}{2} - \frac{Cg^2}{2} + \frac{Cg^2}{3} \right)$$

now taking the derivative of this equation with respect to r

$$4g\tau\mu\ Cr^2 dr = \rho Qr \left(\frac{r\dot{\theta}}{2} - \frac{Cg^2}{2} + \frac{Cg^2}{3}\right)$$

$$C\bar{r}^2 - \left(\frac{Q\rho}{4g\pi W}\right)\left(\bar{r}U - \frac{Cg^2}{6} - (rg^2 r/6)\right) = 0$$

Combining flow variables into non-dimensional groups

$$\frac{Q\rho\ r_o\ g^2}{4g\pi U r_o^2 r_o \theta} = \frac{1}{2} Re R\theta^2$$

dimensionalizing C_o

$$C_o = \frac{r_o \dot{\theta}}{g^2}$$

$$\frac{Q\rho\ g^2}{4g\pi U r_o \theta (6) r_o^2} = \frac{1}{12} Re\ \ \theta^2 Rr$$

$$\frac{Q\rho\ g^2 \bar{r}_o}{4g\pi W r_o^2 r_o} = \frac{1}{12}\ \ Re\ \theta^2\ Rr$$

Thus the above equation reduces to

$$\bar{C}\bar{r}^2 - \frac{1}{2} Re\ R\theta^2 \left(\bar{r} - \frac{1}{6}(C + C_r \bar{r})\right) = 0$$

or

$$\bar{C}_r + \tau\left(\frac{1}{r} + K\bar{r}\right) = 6\text{, where } K = 12/(Re\theta^2 Rr)$$

Solving for $\bar{C}$ by use of U integrating factor

$$\rho = e^{\int P dr} = e^{\int (\frac{1}{\bar{r}} + K\bar{r})dr} = e^{\ln \bar{r} + \frac{K\bar{V}^2}{2}} = \bar{r}\, e^{K\frac{\bar{r}^2}{2}}$$

$$\bar{r}\, e^{\frac{K\bar{r}}{2}} = \int \bar{r} e^{\frac{\bar{K}^2}{2}} (6) + 6$$

$$\rho y = \int Q\, dx + C = \frac{6}{K} \int K\bar{r} e^{\frac{K\bar{r}^2}{2}} + C_o^1$$

$$\int e^U\, dU = e^U$$

$$U = K\bar{r}^2/2$$

$$dU = K\bar{r}$$

$$\bar{r}\, e^{\frac{K\bar{V}^2}{2}} \bar{C} = \frac{6}{K} e^{\frac{K\bar{r}^2}{2}} + C$$

$$\bar{C} = \frac{6}{\bar{r}K} + \frac{1}{\bar{r}} e^{-\frac{\bar{r}^2}{2}} C'_o$$

$$C = \frac{6}{\bar{r}K} + \frac{1}{\bar{r}} e^{-\frac{K\bar{r}^2}{2}} C_o$$

Boundary condition on C.

$$C = 0 \text{ at } \bar{r} = \theta$$

$$0 = \frac{6}{\theta K} + \frac{1}{\theta} e^{-\frac{K\theta^2}{2}} C_o^1$$

$$-\frac{6}{K} e^{\frac{K\theta^2}{2}} = C_o^1$$

Thus $\bar{C}$ is given by:

$$\bar{C} = \frac{6}{\bar{r}K} \left(1 - e^{\frac{K}{2}(\theta^2 - \bar{r}^2)}\right)$$

Non-dimensionalizing shear stress and pressure

$$\tau_s = \mu\, b = \mu\left(\frac{r\dot{\theta}}{g} + cg\right)$$ dimensionalizing shear in

$$\tau_o = \frac{UV_o\theta}{g}$$

$$\tau = \bar{\tau}\,\tau_o = \frac{U\, r_o\dot{\theta}}{g}\,\frac{d\bar{V}}{\alpha\bar{Z}}$$

$$\tilde{\tau} = \mu\left(\frac{\bar{r}_o\theta}{g}\right)\bar{r} - U\,C\,g\,\frac{y}{Ur\theta}$$

$$\bar{\tau} = \bar{r} - \frac{g^2}{r_o\dot{\theta}}\,C$$

$$= \bar{r} - \frac{g^2}{r_o\theta}\,\frac{r_o\dot{\theta}}{y^2}\,C$$

$$\bar{\tau} = \bar{r} - \bar{C}$$ Non-dimensional

Dimensional pressure shear stress

$$P_o = \rho(r_o\dot{\theta})^2$$

$$\frac{dP}{U\bar{r}} = \frac{r_o}{\rho(r_o\dot{\theta})^2}\,\rho\left(\frac{3}{10}\,\frac{r_o\theta^2}{1} - \frac{9g^2}{5\ g^2}\,r_o\theta\right.$$

$$\left.+\ 3\,\bar{C}^2\,\frac{g}{o}\,\frac{U\ r_o^2\theta^2}{r_o\bar{r}\ g^6}\right. - \left.\frac{60\nu}{\pi r_o\bar{r}g^3}\right.$$

$$\frac{d\bar{P}}{d\bar{r}} = \frac{3}{10}\,\bar{r} - \frac{\bar{C}}{5} + \frac{3\bar{C}^2}{70\bar{r}} - 12\,\frac{ReRPV^2}{R}$$

Non-dimensional pressure distribution

VITA

Charles F. Leonard was born on November 22, 1955 in Knoxville, Tennessee. He attended Knoxville Central High School from 1972-74. While in high school he participated in football and in his senior year was elected to the Student Council and also President of the school's Fellowship of Christian Athletes. After graduation from high school he entered The University of Tennessee, Knoxville, in August of that year. During those years at the University he made the Dean's List and became a member of the following professional societies: American Society of Mechanical Engineers, American Society of Heating, Refrigeration and Air-Conditioning Engineers and Pi Tau Sigma. In June of 1978 he graduated from the University with a Bachelor's Degree in Mechanical Engineering, and entered into graduate school in the same department, and graduated with a Master of Science degree in Mechanical Engineering in March, 1980.